

Robustifying Models Against Adversarial Attacks by Langevin Dynamics

Vignesh Srinivasan¹, Arturo Marban^{1,2,3}, Klaus-Robert Müller^{2,3,4,5,*}

Wojciech Samek^{1,3,*} and Shinichi Nakajima^{2,3,6,*}

¹Fraunhofer HHI, ²TU Berlin, ³Berlin Big Data Center,

⁴Korea University, ⁵MPI for Informatics, ⁶RIKEN AIP

{vignesh.srinivasan,wojciech.samek}@hhi.fraunhofer.de

{arturo.marban,klaus-robert.mueller,nakajima}@tu-berlin.de

Abstract

Adversarial attacks on deep learning models have compromised their performance considerably. As remedies, a lot of defense methods were proposed, which however, have been circumvented by newer attacking strategies. In the midst of this ensuing arms race, the problem of robustness against adversarial attacks still remains unsolved. This paper proposes a novel, simple yet effective defense strategy where adversarial samples are relaxed onto the underlying manifold of the (unknown) target class distribution. Specifically, our algorithm drives off-manifold adversarial samples towards high density regions of the data generating distribution of the target class by the Metropolis-adjusted Langevin algorithm (MALA) with *perceptual boundary taken into account*. Although the motivation is similar to projection methods, e.g., Defense-GAN, our algorithm, called MALA for DEfense (MALADE), is equipped with significant dispersion—projection is distributed broadly, and therefore any whitebox attack cannot accurately align the input so that the MALADE moves it to a targeted untrained spot where the model predicts a wrong label. In our experiments, MALADE exhibited state-of-the-art performance against various elaborate attacking strategies.

1 Introduction

Deep neural networks (DNNs) [1, 2, 3, 4, 5] have shown excellent performance in many applications, while they are known to be susceptible to adversarial attacks, i.e., examples crafted intentionally by adding slight noise to the input [6, 7, 8, 9, 10, 11]. These two aspects are considered to be two sides of the same coin: deep structure induces complex interactions between weights of different layers, which provides flexibility in expressing complex input-output relation with relatively small degrees of freedom, while it can make the output function unpredictable in *spots* where training samples exist sparsely. If adversarial attackers manage to find such spots in the input space close to a *real* sample, they can manipulate the behavior of classification, which can lead to a critical risk of security in applications, e.g., self-driving cars, for which high reliability is required.

Different types of defense strategies were proposed, including *adversarial training* [12, 13, 14, 15, 16, 17, 18, 19, 20] which incorporates adversarial samples in the training phase, *projection methods* [16, 21, 22, 23, 24, 25] which denoise adversarial samples by projecting them onto the data manifold, and *preprocessing methods* [26, 27, 28, 29] which try to destroy elaborate spatial coherence hidden in adversarial samples. Although those defense strategies were shown to be robust against the attacking strategies that had been proposed before, most of them have been circumvented by newer attacking strategies. Another type of approaches, called *certification-based methods* [20, 30, 31, 32, 33], minimize (bounds of) the worst case loss over a defined range of perturbations, and provide theoretical guarantees on robustness against any kind of attacks. However, the guarantee holds only for small perturbations, and the performance of those methods against existing attacks are typically inferior to the state-of-the-art. Thus, the problem of robustness against adversarial attacks still remains unsolved.

In this paper, we propose a novel defense strategy, which drives adversarial samples towards high density regions of the data distribution. Fig. 1 explains the idea of our approach. Assume that an attacker

*Asterisks indicate corresponding author

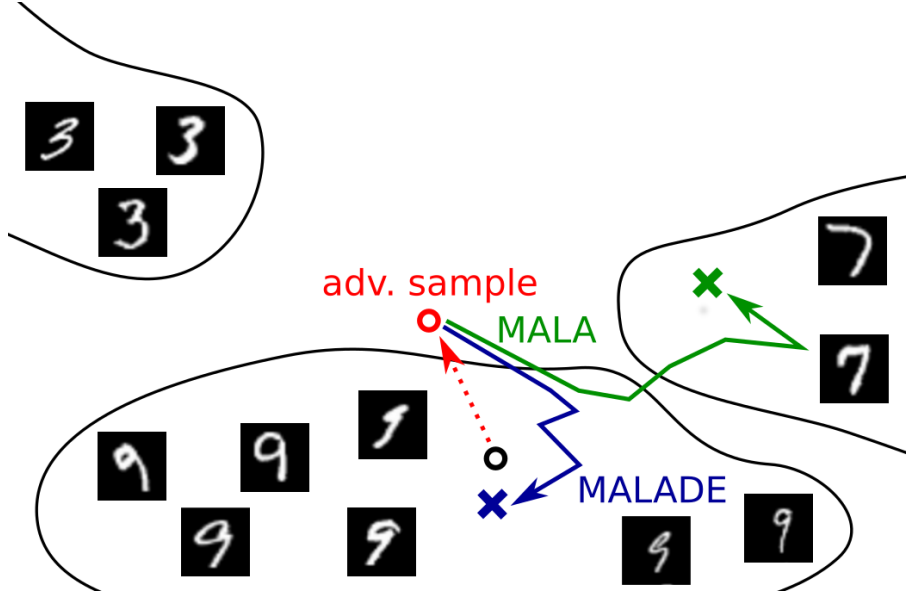


Figure 1: An adversarial sample (red circle) is created by moving the data point (black circle) away from the data manifold, here the manifold of images of digit "9". In this low density area, the DNN is not well trained and thus misclassifies the adversarial sample. Unsupervised sampling techniques such as MALA (green line) project the data point back to high density areas, however, not necessarily to the manifold of the original class. The proposed MALADE (blue line) takes into account of class information and thus projects the adversarial sample back to the manifold of images of digit "9".

created an adversarial sample (red circle) by moving an original sample (black circle) to an *untrained spot* where the target classifier gives a wrong prediction. We can assume that the spot is in a low density area of the training data, i.e., off the data manifold, where the classifier is not well trained, but still close to the original high density area so that the adversarial pattern is imperceptible to a human. Our approach is to *relax* the adversarial sample by Metropolis-adjusted Langevin algorithm (MALA) [34, 35], an efficient Markov chain Monte Carlo (MCMC) sampling method.

MALA requires the gradient of the energy function, which corresponds to the gradient $\nabla_{\mathbf{x}} \log p(\mathbf{x})$ of the log probability, a.k.a., the score function, of the input distribution. However, naively applying MALA would have an apparent drawback: if there exist high density regions (clusters) close to each other but not sharing the same label, MALA could drive a sample into another cluster (see green line in Fig.1), which degrades the classification accuracy. To overcome this drawback, we replace the (marginal) distribution $p(\mathbf{x})$ with the conditional distribution $p(\mathbf{x}|\mathbf{y})$ given label \mathbf{y} . More specifically, our novel defense method, called MALA for DEfense (MALADE), relaxes the adversarial sample based on the conditional gradient $\nabla_{\mathbf{x}} \log p(\mathbf{x}|\mathbf{y})$ by using a novel estimator for the conditional gradient *without knowing the label \mathbf{y} of the test sample*. Thus, MALADE drives the adversarial sample towards high density regions of the data generating distribution for the original class (see blue line in Fig. 1), where the classifier is well trained to predict the correct label.

Our proposed MALADE can be seen as one of the projection methods, most of which have been circumvented by recent attacking methods. However, MALADE has two essential differences from the previous projection methods:

Perceptual boundary taken into account All previous projection methods, including Defense-GAN [23], PixelDefend [22], and others [24, 25], pull the input sample into the closest point on the data manifold without the label information into account. On the other hand, MALADE is designed to drive the input sample into the data manifold of the original class.

Significant dispersion Most projection methods try to pull the adversarial sample back to the original point (so that the adversarial pattern is removed). On the other hand, MALADE drives the input sample to anywhere (randomly) in the closest cluster having the original label. In this sense, MALADE has much larger inherent randomness than the previous projection methods,

Significant dispersion effectively prevents any whitebox attack from aligning the input so that the

MALADE *stably* moves it to a targeted untrained spot, while the awareness of the perceptual boundary keeps the sampling sequence within the cluster with the correct label. Furthermore, it is straightforward to combine MALADE with the state-of-the-art adversarial training method—an advantage to be a projection method—which further boosts the performance.

Our experiments show that MALADE performs comparably to the state-of-the-art methods for older attacks (which had been proposed before the baseline defense methods were proposed) with low perturbation intensity, while it significantly outperforms the state-of-the-art methods for newer attacks or the older attacks with high perturbation intensity. In our experiments, we paid careful attention to the fairness of evaluation, following the recommendation by recent papers [36, 37, 38, 39], where inappropriate evaluation of defense strategies in literature was reported. The authors pointed out that many defense methods were proposed showing good performance against weak versions of attacking strategies, and argued that, when a new defense method is proposed, it should be evaluated thoroughly by appropriately choosing the hyperparameters of attacks, and by elaborating most effective attacks against the proposed defense method. We did our best in this regards, and explored most effective combinations of existing attacking strategies so that the attack is considered to be strongest against our own method.

This paper is organized as follows. We first summarize existing attacking and defense strategies in Section 2. Then, we propose our method with a novel conditional gradient estimator in Section 3. In Section 4, we evaluate our defense method against various attacking strategies, and show advantages over the state-of-the-art defense methods. Section 5 concludes.

2 Existing Methods

In this section, we introduce existing attacking and defense strategies.

2.1 Attacking Strategies

There are two scenarios considered in adversarial attacking. The whitebox scenario assumes that the attacker has the full knowledge on the target classification system, including the architecture and the weights of the DNN and the respective defense strategy,¹ while the blackbox scenario assumes that the attacker has access only to the classifier outputs.

2.1.1 Whitebox Attacks (General)

We first introduce representative whitebox attacks, which are effective against general classifiers with or without defense strategy.

Fast Gradient Sign Method (FGSM) [6] This method is one of the simplest and fastest attacking algorithms. Given an original sample $\mathbf{x} \in \mathbb{R}^L$ and its corresponding label $\mathbf{y} \in \{0, 1\}^K$ in the 1-of- K expression, FGSM creates an adversarial sample by

$$\mathbf{x}' = \mathbf{x} + \varepsilon \cdot \text{sign}(\nabla_{\mathbf{x}} J(\mathbf{x}, \mathbf{y})), \quad (1)$$

where $J(\mathbf{x}, \mathbf{y}) = -\sum_{k=1}^K y_k \log \hat{y}_k(\mathbf{x})$ is the cross entropy loss of the classifier output $\hat{\mathbf{y}} \in [0, 1]^K$ for the true label \mathbf{y} , and ε is the amplitude of adversarial pattern. Eq.(1) effectively reduces the classifier output for the true label, keeping the adversarial sample within the ε -ball around the original sample in terms of the L_∞ -norm.

Projected Gradient Descent (PGD) [17] PGD, a.k.a., the basic iterative method, solves the following problem:

$$\begin{aligned} & \min_{\mathbf{x}'} J(\mathbf{x}', \mathbf{y}) \\ & \text{s.t. } \|\mathbf{x}' - \mathbf{x}\|_p \leq \varepsilon, \quad \mathbf{x}' \in [0, 1]^L, \end{aligned} \quad (2)$$

where $\|\cdot\|_p$ denotes the L_p -norm. This problem can be solved by iterating FGSM (1) as a gradient step and projecting the sample to the allowed set of perturbations. PGD can be seen as an enhanced version of FGSM, and is considered as the strongest first-order attack.

¹ As in [37], we assume that the attacker cannot access to the random numbers (nor random seed) generated and used in stochastic defense processes.

Momentum Iterative fast gradient sign Method (MIM) [40] MIM improves the convergence of the PGD problem (2) by using the momentum, i.e., it iterates

$$\mathbf{x}' = \mathbf{x} + \varepsilon \cdot \text{sign}(\mathbf{g}'), \quad (3)$$

where

$$\mathbf{g}' = \mu \cdot \mathbf{g} + \frac{\nabla_{\mathbf{x}} J(\mathbf{x}, \mathbf{y})}{\|\nabla_{\mathbf{x}} J(\mathbf{x}, \mathbf{y})\|_p},$$

and the projection step.

Carlini-Wagner (CW) [41] The CW attack optimizes the adversarial pattern $\boldsymbol{\tau} \in \mathbb{R}^L$ by solving

$$\begin{aligned} \min_{\boldsymbol{\tau}} & \|\boldsymbol{\tau}\|_p + c \cdot F(\mathbf{x} + \boldsymbol{\tau}, \mathbf{y}) \\ \text{s.t.} & \quad \mathbf{x} + \boldsymbol{\tau} \in [0, 1]^L, \end{aligned} \quad (4)$$

where

$$\begin{aligned} F(\mathbf{x} + \boldsymbol{\tau}, \mathbf{y}) = & \max\{0, \log \hat{y}_{k^*}(\mathbf{x} + \boldsymbol{\tau}) \\ & - \max_{k \neq k^*} \log \hat{y}_k(\mathbf{x} + \boldsymbol{\tau}) + \iota\}. \end{aligned}$$

Here, c is a trade-off parameter balancing the pattern intensity and the adversariality, k^* is the true label id, i.e., $y_{k^*} = 1$, and ι is a margin for the sample to be adversarial.

Elastic-net Attack to Deep neural networks (EAD) [42, 43] EAD is a modification of the CW attack where the L_p regularizer is replaced with the elastic-net regularizer, the sum of l_1 - and l_2 -norms:

$$\begin{aligned} \min_{\boldsymbol{\tau}} & \beta \|\boldsymbol{\tau}\|_1 + \|\boldsymbol{\tau}\|_2 + c \cdot F(\mathbf{x} + \boldsymbol{\tau}, \mathbf{y}) \\ \text{s.t.} & \quad \mathbf{x} + \boldsymbol{\tau} \in [0, 1]^L, \end{aligned} \quad (5)$$

where β is a parameter controlling the sparsity. This method creates sparse adversarial patterns, and has shown to be very effective against the classifiers that are protected against dense, e.g., L_∞ -bounded, adversarial patterns.

2.1.2 Whitebox Attacks (Specialized)

Some attacking strategies target specific features of defense strategies, and enhance general whitebox attacks (introduced in the previous subsection). Here we introduce strategies that are considered to be effective for attacking our defense method, which will be proposed in Section 3.

Reconstruction (R) Regularization [44] Some defense strategies are equipped with a denoising process, where adversarial pattern is removed by projection, e.g., by an autoencoder. The R regularization is designed to disarm those defense strategies by finding a point which is unaffected by the denoising process. In the original work, called R+PGD [44], the sum of the reconstruction loss by the denoising process and the (negative) cross entropy loss is minimized.

Back Pass Differentiable Approximation (BPDA) [37] Many defense strategies, explicitly or implicitly, rely on *gradient obfuscation*, which prevents whitebox attackers from stably computing the gradient, e.g., by having non-differentiable layers or artificially inducing randomness. BPDA simply replaces such layers with identity maps, in order to stably estimate the gradient. This method is effective when the replaced layer is the denoising process that reconstructs the original input well, so that $\nabla_{\mathbf{x}} \hat{y}_k(r(\mathbf{x}')) \approx \nabla_{\mathbf{x}} \hat{y}_k(\mathbf{x})$ holds.

Expectation over Transformation (EOT) [37] The EOT method estimates the gradient by averaging over multiple trails, so that the randomness is averaged out. This method is effective against any stochastic defense methods.

2.1.3 Blackbox Attacks

Blackbox attacks are, by definition, weaker than whitebox attacks. Here we introduce a few of them.

Distillation Attack [7, 45] One can apply any whitebox method after knowledge distillation, where a student network is trained from classifier outputs. Distillation attacks are, in principle, weaker than the corresponding whitebox attacks.

Boundary Attack [46] This method first finds an initial adversarial point \mathbf{x}'_0 by random search. Specifically, it adds uniform noise to the original sample until the sample becomes adversarial, i.e., $\hat{\mathbf{y}}(\mathbf{x}'_0) \neq \mathbf{y}$. Once a initial point is found, it iterates a random search step to reduce the norm of the adversarial pattern. In each iteration, random exploration first finds the perceptual boundary on the sphere that is centered at the original sample \mathbf{x} , and contains the current point \mathbf{x}'_t . Based on the boundary information, the point is moved towards the original sample so that the distance to the original sample is reduced, i.e., $\|\mathbf{x}'_{t+1} - \mathbf{x}\|_p < \|\mathbf{x}'_t - \mathbf{x}\|_p$, while the adversariality is kept, i.e., $\hat{\mathbf{y}}(\mathbf{x}'_{t+1}) \neq \mathbf{y}$. This process is iterated T times.

Salt and Pepper Noise Attack [47] This method corrupts the original image with a fixed amount of impulsive salt and pepper noise. The number of corrupted pixels is bounded by ρL for $0 < \rho \leq 1$. It was reported that the sharp discontinuity of the salt and pepper noise enables strong adversarial attack, bringing down the classification accuracy significantly [47].

Transfer Attack [48] Assume that the attacker has full access to another classifier which was trained for the same purpose (possibly equipped with some defense strategy) as the target classifier. Then, the attacker can create adversarial samples by any whitebox attack against the known model, and use them to attack the target classifier. This attack can be considered as blackbox.

2.2 Defense Strategies

As mentioned in Section 1, existing methods can be roughly classified into four categories.

Adversarial Training In this strategy, adversarial samples are generated by known attacking strategies, and added to the training data, in order to make the classifier robust against those attacks [7, 15, 16, 17, 18, 19, 20, 49]. The method [17] proposed by Madry et al. (2017), which we refer to as "Madry" in this paper, withstood many adversarial attacks, and is considered to be the current state-of-the-art defense strategy that outperforms most of the other existing defense methods against most of the attacking methods. Adversarial Logit Pairing (ALP) [18] uses adversarial samples during training while performing logit pairing between adversarial samples and original samples thereby pulling the logits of the adversarial sample to be as similar as possible to the original. Although it was found [36] that ALP is not as robust as what the original paper reported, it is still considered to be one of the state-of-the-art methods.

Methods in this category, typically show higher robustness than methods in the other categories. However, they have a risk of overfitting to the known attacking strategies [42, 43] and to intensity of perturbations [17]. Our experiments in Section 4 reveal this weakness of adversarial training—Madry performs very well against FGSM [6], PGD [17], CW [41], and MIM [40], while it was broken down by EAD [42, 43], which was proposed after Madry was proposed.

Projection Methods Generative models have been shown to be useful to reconstruct the original image (or to remove the adversarial patterns) from an adversarial sample [23, 24, 25]. Defense-GAN [23] searches over the latent space of a generative adversarial network (GAN), and provides a generated sample closest to the input as a reconstruction of the original image. Since the generative model is trained to generate samples in the data manifold, Defense-GAN effectively projects off-manifold sample onto the data manifold. Similarly, PixelDefend [22] employs PixelCNN to project the adversarial image back to the training distribution. [24] proposed an untrained generative network as a deep image prior to reconstruct the original image. The Analysis By Synthesis (ABS) method [21] uses a variational autoencoder to find the optimal latent vector maximizing the lower bound of the log likelihood of the given input to each of the class.

Most existing strategies in this category have been rendered as ineffective against recent attacking strategies: Defense-GAN and PixelDefend have been broken down by BPDA [37].

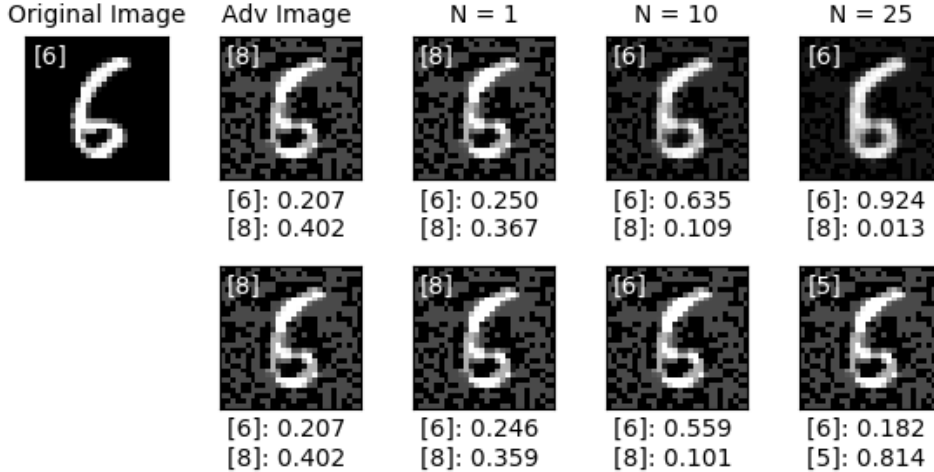


Figure 2: The top-left is the original image, from which the adversarial image (second column) was crafted. The third to the fifth columns show the images after $N = 1, 10,$ and 25 steps of MALADE (top-row) and of MALA with the marginal distribution (bottom-row). Below each image, the prediction output \hat{y}_{k^*} for the original label $k^* = "6"$ and that for the label with the highest output, i.e., $k = \operatorname{argmax}_{k \neq k^*} \hat{y}_k$, are shown. In this example, MALADE, trained with perceptual information, drove the adversarial sample towards the right cluster with the original label "6". On the other hand, although MALA successfully removed the adversarial pattern for "8", it brought the sample into a neighboring cluster with a wrong label "5".

Preprocessing Methods Preprocessing was known to be effective for adversarial defense. Specifically, it was reported that image transformations (e.g., bit depth reduction, JPEG compression and decompression, random padding) can destroy elaborate spatial coherence hidden in adversarial samples [26, 29, 50]. However, [37] showed that this kind of defense strategies can be easily broken down by BPDA or EOT. Autoencoders can also be used as a preprocessor to remove adversarial patterns [27, 28], which however were broken down by CW [51].

The methods in this category are generally seen as weaker than those in the other categories.

Certification-based Methods Certification-based methods employ robust optimization, and obtain *provably robust* networks. The idea is to train the classifier by minimizing (upper-bounds of) the worst-case loss over a defined range of perturbations, so that creating adversarial samples in the range is impossible. To this end, one needs to solve a nested optimization problem, which consists of the inner optimization finding the worst case sample (or the strongest adversarial sample) and the outer optimization minimizing the worst-case loss. Since the inner optimization is typically non-convex, different relaxations [30, 31, 32, 33, 52] have been applied for scaling this approach.

The certification-based approach seems a promising direction towards the end of the arms race—it might protect classifiers against any (known or unknown) attacking strategy in the future. However, the existing methods still have limitations in many aspects, e.g., structure of networks, scalability, and the guaranteed range of the perturbation intensity. Typically, the robustness is guaranteed only for small perturbations, e.g., $\varepsilon = 0.1 L_\infty$ -bound in MNIST [31, 32, 33], and no method in this category has shown comparable performance to the state-of-the-art.

3 Proposed Method

In this section, we propose our novel defense strategy, which drives the input sample (if it lies in low density regions) towards high density regions. We achieve this by using Langevin dynamics.

Metropolis-adjusted Langevin Algorithm (MALA) MALA is an efficient Markov chain Monte Carlo (MCMC) sampling method which uses the gradient of the energy (negative log-probability $E(\mathbf{x}) = -\log p(\mathbf{x})$). Sampling is performed sequentially by

$$\mathbf{x}_{t+1} = \mathbf{x}_t + \alpha \nabla_{\mathbf{x}} \log p(\mathbf{x}_t) + \kappa, \quad (6)$$

where α is the step size, and $\boldsymbol{\kappa}$ is random perturbation subject to $\mathcal{N}(\mathbf{0}, \delta^2 \mathbf{I}_L)$. By appropriately controlling the step size α and the noise variance δ^2 , the sequence is known to converge to the distribution $p(\mathbf{x})$.²

We estimate the gradient, the second term in Eq.(6), by using a denoising autoencoder (DAE) [54]. Let $\mathbf{r} : \mathbb{R}^L \mapsto \mathbb{R}^L$ be a function that minimizes

$$\mathbb{E}_{p'(\mathbf{x})p'(\boldsymbol{\nu})} [\|\mathbf{r}(\mathbf{x} + \boldsymbol{\nu}) - \mathbf{x}\|^2], \quad (7)$$

where $\mathbb{E}_p[\cdot]$ denotes the expectation over the distribution p , $\mathbf{x} \in \mathbb{R}^L$ is a training sample subject to a distribution $p(\mathbf{x})$, and $\boldsymbol{\nu} \sim \mathcal{N}_L(\mathbf{0}, \sigma^2 \mathbf{I})$ is an L -dimensional artificial Gaussian noise with mean zero and variance σ^2 . $p'(\cdot)$ denotes an empirical (training) distribution of the distribution $p(\cdot)$, namely, $\mathbb{E}_{p'(\mathbf{x})}[g(\mathbf{x})] = N^{-1} \sum_{n=1}^N g(\mathbf{x}^{(n)})$ where $\{\mathbf{x}^{(n)}\}_{n=1}^N$ are the training samples.

Proposition 1 [55] *Under the assumption that $\mathbf{r}(\mathbf{x}) = \mathbf{x} + o(1)$ ³, the minimizer of the DAE objective (7) satisfies*

$$\mathbf{r}(\mathbf{x}) - \mathbf{x} = \sigma^2 \nabla_{\mathbf{x}} \log p(\mathbf{x}) + o(\sigma^2), \quad (8)$$

as $\sigma^2 \rightarrow 0$.

Proposition 1 states that a DAE trained with a small σ^2 can be used to estimate the gradient of the log probability. In a blog [56], it was proved that the residual is proportional to the score function of the noisy input distribution for any σ^2 , i.e.,

$$\mathbf{r}(\mathbf{x}) - \mathbf{x} = \sigma^2 \nabla_{\mathbf{x}} \log \int \mathcal{N}_L(\mathbf{x}; \mathbf{x}', \sigma^2 \mathbf{I}_L) p(\mathbf{x}') d\mathbf{x}'. \quad (9)$$

MALA for Defense (MALADE) As discussed in Section 1, MALA drives the input into high density regions but not necessarily to the cluster sharing the same label with the original image (see Fig. 1). To overcome this drawback, we propose MALA for defence (MALADE), where samples are relaxed based on the *conditional* training distribution $p(\mathbf{x}|\mathbf{y})$, instead of the marginal $p(\mathbf{x})$. More specifically, sampling is performed by

$$\mathbf{x}_{t+1} = \mathbf{x}_t + \alpha \mathbb{E}_{p(\mathbf{y}|\mathbf{x}_t)} [\nabla_{\mathbf{x}} \log p(\mathbf{x}_t|\mathbf{y})] + \boldsymbol{\kappa}. \quad (10)$$

Fig 2 shows a typical example, where MALADE (top-row) successfully drives the adversarial sample to the correct cluster, while MALA (bottom-row) drives it to a wrong cluster.

To estimate the second term in Eq.(10), we train a supervised variant of DAE, which we call a supervised DAE (sDAE), by minimizing

$$\mathbb{E}_{p'(\mathbf{x}, \mathbf{y})p'(\boldsymbol{\nu})} \left[\|\mathbf{r}(\mathbf{x} + \boldsymbol{\nu}) - \mathbf{x}\|^2 - 2\sigma^2 J(\mathbf{r}(\mathbf{x} + \boldsymbol{\nu}), \mathbf{y}) \right]. \quad (11)$$

The difference from the DAE objective (7) is in the second term, which is proportional to the cross entropy loss. With this additional term, sDAE provides the gradient estimator of the log-*joint*-probability $\log p(\mathbf{x}, \mathbf{y})$ averaged over the conditional training distribution.

Theorem 1 *Assume that the classifier output accurately reflects the conditional probability of the training data, i.e., $\hat{\mathbf{y}}(\mathbf{x}) = p(\mathbf{y}|\mathbf{x})$, then the minimizer of the sDAE objective (10) satisfies*

$$\mathbf{r}(\mathbf{x}) - \mathbf{x} = \sigma^2 \mathbb{E}_{p(\mathbf{y}|\mathbf{x})} [\nabla_{\mathbf{x}} \log p(\mathbf{x}, \mathbf{y})] + O(\sigma^3). \quad (12)$$

(Sketch of proof) Similarly to the analysis in [55], we first Taylor expand $\mathbf{r}(\mathbf{x} + \boldsymbol{\nu})$ around \mathbf{x} , and approximate the sDAE objective (11) by a function similar to the objective for contractive autoencoder (CAE). Applying the second order Euler-Lagrange equation to the approximate objective gives Eq.(12) as a stationary condition. The complete proof is given in Appendix A. \square

² For convergence, a rejection step after Eq.(6) is required. However, it was observed that a variant, called MALA-approx [53], without the rejection step gives reasonable sequence for moderate step sizes. We use MALA-approx in our proposed method.

³ This assumption is not essential as we show in the proof in Appendix A.

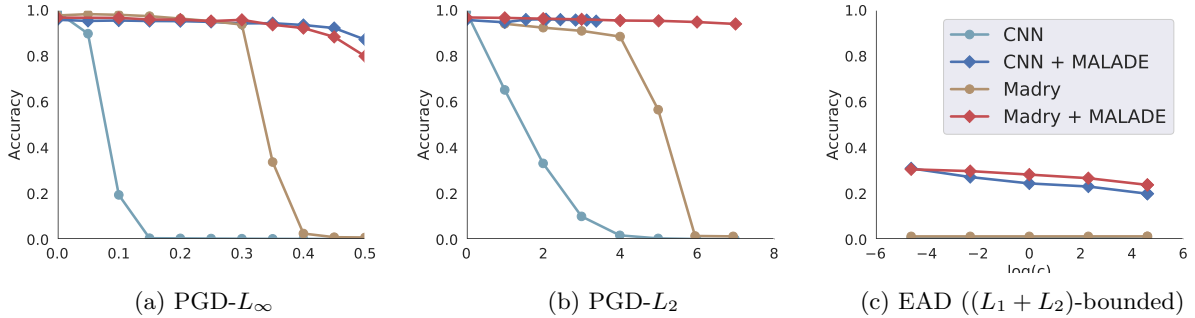


Figure 3: Classification accuracy on MNIST against (a) PGD- L_∞ , (b) PGD- L_2 , and (c) EAD attacks. The curves correspond to the original convolutional neural network (CNN) classifier, the CNN classifier protected by MALADE (CNN+MALADE), the Madry classifier [17], and the Madry classifier protected by MALADE (Madry+MALADE). In each plot, the horizontal axis indicates the intensity of the adversarial perturbations, i.e., ε for PGD and $\log c$ for EAD. All plots show that MALADE significantly boosts the robustness of both classifiers.

Since $p(\mathbf{x}, \mathbf{y}) = p(\mathbf{x}|\mathbf{y})p(\mathbf{y})$, if the label distribution is flat (or equivalently the number of training samples for all classes is the same), i.e., $p(\mathbf{y}) = 1/K$, the residual of sDAE gives an estimator for the second term in Eq.(10):

$$\mathbf{r}(\mathbf{x}) - \mathbf{x} = \sigma^2 \mathbb{E}_{p(\mathbf{y}|\mathbf{x})} [\nabla_{\mathbf{x}} \log p(\mathbf{x}|\mathbf{y})] + O(\sigma^3).$$

The term $\mathbb{E}_{p(\mathbf{y}|\mathbf{x})} [\nabla_{\mathbf{x}} \log p(\mathbf{x}|\mathbf{y})]$ is the gradient of the log-*conditional*-distribution on the label, where the label is estimated from the prior knowledge (the expectation is taken over the training distribution of the label, given \mathbf{x}). If the number of training samples are non-uniform over the classes, the weight (or the step size) should be adjusted so that all classes contribute equally to the training.

As discussed in Section 1, MALADE falls into the category of projection methods, in which most existing methods are outperformed by strong adversarial training methods. Nevertheless, our experiment in Section 4 shows its comparable (or even better under some conditions) performance than Madry [17], the state-of-the-art adversarial training method. We suppose that this is because of its inherent randomness—MALADE drives an input not always to the neighborhood of the original point (i.e., the point before the adversarial pattern was added), but any point in the cluster sharing the same label with the original image. This large stochasticity prevents the attacker from aligning the input so that the MALADE *stably* moves it to a targeted untrained spot where the model predicts a wrong label.

Adversarial training methods effectively fill untrained spots close to the data manifold with additional training samples, so that those weak spots of the classifier are removed. On the other hand, MALADE prevents samples from being classified at any untrained spot. These two approaches are orthogonal and can naturally be combined: In the training phase, adversarial training fills most untrained spots with additional samples, and, in the test phase, MALADE prevents the classifier from making prediction at any untrained spot even if adversarial training failed to remove all of them. Our experiment in Section 4 shows that this combination outperforms all existing defense methods.

4 Experiments

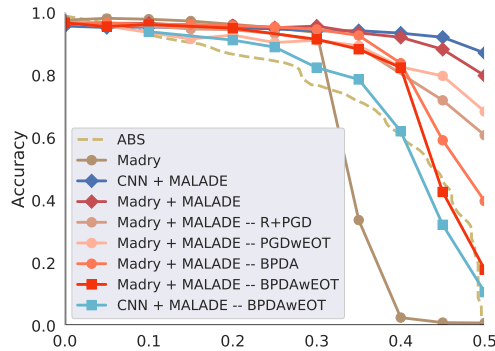
In this section, we empirically evaluate our proposed MALADE against various attacking strategies, and compare it with the state-of-the-art baseline defense strategies.

4.1 Datasets

We conduct experiments on the following datasets:

MNIST: MNIST consists of handwritten digits from 0-9. The dataset is split into training, validation and test set with 50,000, 10,000 and 10,000 images, respectively. MNIST, in spite of being a small dataset, remains to be considered as adversarially robust.

CIFAR10: CIFAR10 consists of natural images for 10 classes. The resolution is $32 \times 32 \times 3$, and the dataset defines 50,000 training images and 10,000 test images.



(a) PGD- L_∞

Figure 4: Classification accuracy on MNIST against the attacks adapted for our proposed MALADE. The adversarial samples were created by PGD- L_∞ enhanced with R regularization, BPDA, and EOT, respectively. Although the adapted attacks reduce accuracy of MALADE, Madry+MALADE still performs better than the baselines (Madry and ABS).

TinyImagenet: TinyImagenet is a subset of the large Imagenet dataset consisting of 200 classes out of the 1000 classes. Each class contains 500 training images and 50 test images. The images are subsampled to have a resolution of $64 \times 64 \times 3$.

4.2 Attacking Strategies

We evaluate defense methods against the following attacking strategies:

Whitebox Attacks: We chose PGD [57], CW [58], MIM [46], and EAD [59] as state-of-the-art whitebox attacks. Indeed they have broken down many recent defense strategies [37], and MIM is the winner of NIPS 2017 competition on adversarial attacks [40].

Blackbox Attacks: We chose Boundary Attack [46] and Salt and Pepper Attack [47] as state-of-the-art blackbox attacks. We omit distillation attacks [7, 45] because they are in principle weaker than the corresponding whitebox attacks. We add Transfer Attack [48] under the blackbox scenario, where the attackers craft the data on different defense strategies.

In our experiment, we pay careful attention to *fairness* of evaluation. Recent papers [36, 37, 38, 39] reported on inappropriate evaluation of defense strategies in literature. Most of the cases, attacking samples were created with inappropriate parameter setting, e.g., the maximum number of iterations is too small to converge, or attacking methods were not properly *adapted* so that they are effective to the proposed defense method. To avoid this, we first make sure that the attacking methods are applied with appropriate parameter setting. Specifically, we set the maximum number of iterations to a sufficient large value, and confirm the convergence (see Appendix B.1). Furthermore, we explore possible attacking methods suitable against our proposed MALADE, by combining following ideas with the general whitebox strategies:

Whitebox Attacks adapted to MALADE: We consider R regularization [44], BPDA [37], and EOT [37] to be suitable strategies for breaking down MALADE, which is equipped with stochastic denoising (projection) step. They are used in combination with general whitebox attacks, e.g., R+PGD, PGD with EOT (PGDwEOT), etc.

4.3 Baseline Defense Strategies

We choose two adversarial training methods, Madry [17] and ALP [18], as the state-of-the-art baseline defense methods to be compared with our proposed MALADE. Due to the availability of pretrained networks, we evaluate Madry on MNIST and CIFAR10,⁴ and ALP on TinyImagenet.⁵

⁴https://github.com/tensorflow/models/tree/master/research/adversarial_logit_pairing

⁵https://github.com/MadryLab/mnist_challenge

Table 1: Summary of classification performance on MNIST. For each attacking scenario, i.e., white-box/blackbox and bounds for the amplitude of adversarial patterns, the lowest row gives the *worst case* result over the considered attacking strategies.

Setting	Condition	Attack	CNN	Madry	CNN + MALADE	Madry + MALADE
<i>whitebox</i>	L_∞ $\varepsilon = 0.3$	FGSM	11.77	97.52	93.54	95.59
		PGD	0.00	93.71	94.22	95.76
		R+PGD	-	-	92.65	93.51
		BPDA	-	-	84.74	94.70
		BPDAwEOT	-	-	82.48	91.54
		MIM	0.00	97.66	94.32	94.53
		<i>worst case</i>	0.00	93.71	82.48	91.54
	L_∞ $\varepsilon = 0.4$	PGD	0.00	0.02	93.51	92.18
		BPDA	-	-	66.16	83.90
		BPDAwEOT	-	-	62.15	80.65
		<i>worst case</i>	0.00	0.02	62.15	80.65
	L_2 $\varepsilon = 4$	FGM	30.79	97.68	94.68	96.05
		PGD	0.01	92.68	95.91	96.76
		CW	0.00	85.53	90.07	91.14
		<i>worst case</i>	0.0	85.53	90.07	91.14
L_2-L_1 $\beta = 0.01$ and $c = 0.01$	EAD	0.00	0.01	31.00	30.59	
<i>blackbox</i>	$\rho = 0.25$ $T = 5,000$	SaltnPepper	36.49	41.61	80.41	80.72
		Boundary Attack	32.39	1.10	93.79	95.80
		<i>worst case</i>	32.39	1.10	80.41	80.72

4.4 Results on MINST

We first show our extensive experiments on MNIST. Fig. 3 shows classification accuracy of the original convolutional neural network (CNN) classifier, the CNN classifier protected by MALADE (CNN+MALADE), the Madry classifier, i.e., the classifier trained with adversarial samples, and the Madry classifier protected by MALADE (Madry+MALADE). The adversarial samples were created by (a) PGD- L_∞ , (b) PGD- L_2 , and (c) EAD attacks, where PGD- L_p denotes the L_p -bounded PGD attack. Note that EAD can be seen as an $(L_1 + L_2)$ -bounded attack, producing sparse adversarial patterns. In each plot in Fig. 3, the horizontal axis indicates to the intensity of the adversarial perturbations, i.e., ε for PGD and $\log c$ for EAD. The Madry classifier was trained on the adversarial samples created by PGD- L_∞ for $\varepsilon = 0.3$.

As expected, Madry is robust against PGD- L_∞ up to $\varepsilon \leq 0.3$. Consistently with the author’s report [17], it is also robust against PGD- L_2 up to $\varepsilon \leq 4.5$. However, Madry is broken down by PGD- L_∞ for $\varepsilon > 0.4$ and PGD- L_2 for $\varepsilon > 6$. Furthermore, EAD, which was proposed more recently than Madry, completely breaks down Madry. On the other hand, our proposed MALADE is robust against PGD- L_∞ and PGD- L_2 in a wide range of ε , and is not completely broken down by EAD.

Next, we investigate the robustness against attacking strategies, which we elaborated for attacking our own method. Fig. 4 shows the performance of Madry+MALADE against PGD- L_∞ enhanced by R regularization, BPDA, and EOT, respectively, which are considered to be effective against MALADE. For comparison, we show the performance of Madry and ABS [21] against the plain PGD- L_∞ . We see that, although the elaborated attacks reduce the accuracy of Madry+MALADE to some extent, their effect is limited, and even in the worst case, i.e., against BPDA with EOT (BPDAwEOT), Madry+MALADE performs better than the baseline methods, i.e., Madry and ABS. The effect of EOT is visualized in Fig.7 in Appendix.

Table 1 summarizes classification performance of defense strategies against various attacks. For each attacking scenario, i.e., whitebox/blackbox and bounds for the amplitude of adversarial patterns, the lowest row gives the *worst case* result over the considered attacking strategies, which should be seen as a robustness criterion of defense strategy—a good defense method must be robust against any attacking strategy.

Madry performs best under the whitebox scenario with L_∞ -bounded adversary for $\varepsilon = 0.3$ —the setting against which Madry was trained to be robust. However, Madry+MALADE shows comparable performance under this setting. For the other cases including larger ε and different norm bounds,

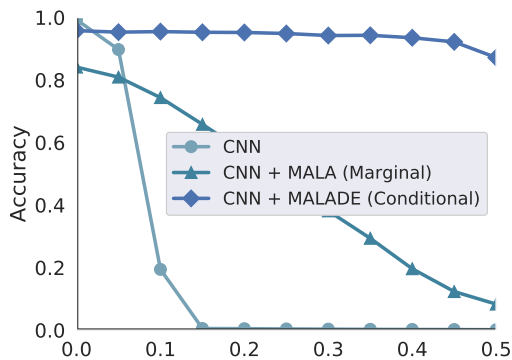
Table 2: Classification performance on MNIST under the transfer attack with L_∞ -bounded adversary for $\varepsilon = 0.4$. The columns correspond to the classifiers of which the robustness is measured, while the rows corresponds to the classifiers against which the adversarial samples are crafted. The bottom row shows the *worst case* result for defender, i.e., the most successful attack by an attacker who has full knowledge on the three other classifiers other than the target classifier.

	CNN	Madry	CNN + MALADE	Madry + MALADE
CNN	-	81.20	90.11	92.84
Madry	26.92	-	76.87	73.69
CNN + MALADE	9.19	77.55	-	71.40
Madry + MALADE	26.12	63.47	78.20	-
<i>worst case</i>	9.19	63.47	76.87	71.40

Madry+MALADE, as well as CNN+MALADE, significantly outperforms Madry.

Table 1 also shows results under the blackbox scenario with the state-of-the-art attacking strategies, SaltNPepper and Boundary attack. The table clearly shows high robustness of MALADE against those attacks, while Madry exhibits its vulnerability against them.

Table 2 evaluates robustness of the four classifiers, CNN, Madry, CNN+MALADE, and Madry+MALADE, against transfer attacks. Assume for example that, when CNN is attacked, the attacker has full knowledge on Madry, CNN+MALADE, and Madry+MALADE but not on CNN.⁶ In such a case, a reasonable strategy for the attacker is to craft adversarial samples against each of the known classifiers, i.e., Madry, CNN+MALADE, and Madry+MALADE, and use them to attack the target classifier, i.e., CNN. This particular example corresponds to the second column of Table 2, where the bottom row shows the *worst case* result for the defender, i.e., the most successful attack. For the attacking method, the strongest one in Table 1 was chosen, i.e., PGD when adversarial samples are crafted against CNN and Madry, and BPDawEOT when adversarial samples are crafted against CNN+MALADE and Madry+MALADE. Also in this transfer attack scenario, we see that our MALADE outperforms the state-of-the-art Madry classifier.



(a) PGD- L_∞

Figure 5: Comparison between MALADE and MALA (with marginal distribution). The superiority of MALADE to MALA (marginal) is clearly seen, which proves the benefit of using perceptual boundary information in driving adversarial samples into high density areas.

Summarizing our experimental results on MNIST, our proposed MALADE showed excellent performance under different attacking scenarios, and different threat models (bounds for adversarial patterns). Adversarial examples crafted by various strategies can be found in Appendix D.

Before moving to experiments on larger scale data, we show the importance of our new development,

⁶This includes the case that the attacker simply does not know that the target classifier is the plain CNN.

Table 3: Summary of classification performance on CIFAR10. For PGD attack, the number of steps was fixed at 100. For blackbox attacking scenario, the lowest row gives the *worst case* result over the considered attacking strategies.

Setting	Condition	Attack	CNN	Madry	CNN + MALADE	Madry + MALADE
<i>whitebox</i>	$L_\infty \ \varepsilon = 8$	PGD	0.00	32.86	0.48	33.89
	$L_\infty \ \varepsilon = 16$	PGD	0.00	10.28	0.16	11.46
<i>blackbox</i>	$\rho = 0.05$ $T = 10,000$	SaltnPepper	13.54	11.09	15.19	11.12
		Boundary Attack	12.76	34.97	17.72	73.57
	<i>worst case</i>		12.76	11.09	15.19	11.12

Table 4: Summary of classification performance on TinyImagenet. For PGD attack, the number of steps was fixed at 100. For blackbox attacking scenario, the lowest row gives the *worst case* result over the considered attacking strategies.

Setting	Condition	Attack	CNN	ALP	CNN + MALADE	ALP + MALADE
<i>whitebox</i>	$L_\infty \ \varepsilon = 1$	PGD	9.49	27.05	10.07	31.80
	$L_\infty \ \varepsilon = 4$	PGD	0.20	12.78	0.26	13.23
<i>blackbox</i>	$\rho = 0.05$ $T = 10,000$	SaltnPepper	2.45	9.91	6.23	9.94
		Boundary Attack	9.12	7.38	63.54	44.35
	<i>worst case</i>		2.45	7.38	6.23	9.94

i.e., sDAE providing the gradient for the conditional distribution $p(\mathbf{x}|\mathbf{y})$. To this end, we compare in Fig. 5 the classification accuracy of MALADE and MALA (with marginal distribution $p(\mathbf{x})$) against PGD- L_∞ . MALA (marginal) shows robustness against adversarial attack with high intensity (compared to the original CNN classifier). However, the lack of perceptual boundary information clearly degrades the performance, and thus MALA (marginal) is significantly outperformed by MALADE over all intensity range. This supports our initial hypothesis explained in Fig.1—MALA drives a sample to a neighboring cluster which does not necessarily share the correct label—and imply that cases similar to the example shown in Fig.2 often happen.

4.5 Results on CIFAR10 and TinyImagenet

Here we apply our defense strategy for larger datasets. Tables 3 and 4 report on classification accuracy on CIFAR10 and on TinyImagenet, respectively, against whitebox (PGD- L_∞) and blackbox (SaltnPepper and Boundary) attacks. On TinyImagenet, we show the performance of ALP [18] as the baseline defense method. Similarly to Madry+MALADE, it is straightforward to combine MALADE and ALP to form ALP+MALADE.

Overall, classification accuracy is not high, which reflects the fact that the state-of-the-art has not achieved satisfactory level of robustness against adversarial attacks in the scale of CIFAR10 and TinyImagenet datasets. However, the observation that MALADE consistently improves the robustness of classifiers implies that our approach is a hopeful direction for solving the issue of defense against adversarial attacks in large scale problems.

5 Conclusion

Adversarial attacks against deep learning models change a sample so that human perception does not allow to detect the change. However, the classifier is compromised and yields a false prediction. Many defense strategies attempted to alleviate this effect by pre-processing, projection, adversarial training, or robust optimization. However most of the defenses have been broken down by newer attacks or variations of existing attacks.

In this work, we have proposed to use the Metropolis-adjusted Langevin algorithm (MALA) which is guided through a supervised DAE—MALA for DEfense (MALADE). This framework allows us to drive adversarial samples towards the underlying data manifold and thus towards the high density regions

of the data generating distribution, where the nonlinear learning machine is supposed to be trained well with sufficiently many training data. In this process, the gradient is computed not based on the *marginal* input distribution but on the *conditional* input distribution given output, and it is estimated by a novel supervised DAE. This prevents MALADE from driving samples into a neighboring cluster with a wrong label, and gives rise to high generalization performance that significantly reduces the effect of adversarial attacks. We have empirically showed that MALADE is fairly robust—it compares favorably or significantly outperforms the state-of-the-art defense methods [17, 18] under different adversarial scenarios and attacking strategies.

Supposing that the difficulty lies in the complex structure of untrained spots close to the data manifold, which increases along with the increase in data size and complexity of the model, we see MALADE as a hopeful defence strategy, which effectively removes a lot of untrained spots simultaneously without using additional training samples to fill those spots one by one. However, further efforts must be made, e.g., in stabilizing the prediction by majority voting from a collection of the generated samples after burn-in, and in developing tools which robustly estimate the gradient in high dimensional space, which are left as future work. Other future work includes analyzing the attacks and defenses using interpretation methods [60, 61], and applying the supervised DAE to other applications such as federated or distributed learning [62, 63].

Acknowledgments

This work was supported by the Fraunhofer Society under the MPI-FhG collaboration project “Theory & Practice for Reduced Learning Machines”. This work was also supported by the German Ministry for Education and Research (BMBF) as Berlin Big Data Center (01IS18025A) and Berlin Center for Machine Learning (01IS18037I), the German Research Foundation (DFG) as Math+: Berlin Mathematics Research Center (EXC 2046/1, project-ID: 390685689), and the Information & Communications Technology Planning & Evaluation (IITP) grant funded by the Korea government (No. 2017-0-00451, No. 2017-0-01779).

References

- [1] Alex Krizhevsky, Ilya Sutskever, and Geoffrey E Hinton. Imagenet classification with deep convolutional neural networks. In *Advances in neural information processing systems*, pages 1097–1105, 2012.
- [2] Yann LeCun, Léon Bottou, Yoshua Bengio, and Patrick Haffner. Gradient-based learning applied to document recognition. *Proceedings of the IEEE*, 86(11):2278–2324, 1998.
- [3] C. Szegedy, Wei Liu, Yangqing Jia, P. Sermanet, S. Reed, D. Anguelov, D. Erhan, V. Vanhoucke, and A. Rabinovich. Going deeper with convolutions. In *2015 IEEE Conference on Computer Vision and Pattern Recognition (CVPR)*, pages 1–9, June 2015.
- [4] Karen Simonyan and Andrew Zisserman. Very deep convolutional networks for large-scale image recognition. *arXiv preprint arXiv:1409.1556*, 2014.
- [5] Kaiming He, Xiangyu Zhang, Shaoqing Ren, and Jian Sun. Deep residual learning for image recognition. In *Proceedings of the IEEE conference on computer vision and pattern recognition*, pages 770–778, 2016.
- [6] Ian J Goodfellow, Jonathon Shlens, and Christian Szegedy. Explaining and harnessing adversarial examples. *arXiv preprint arXiv:1412.6572*, 2014.
- [7] Nicolas Papernot, Patrick McDaniel, Ian Goodfellow, Somesh Jha, Z Berkay Celik, and Ananthram Swami. Practical black-box attacks against machine learning. In *Proceedings of the 2017 ACM on Asia Conference on Computer and Communications Security*, pages 506–519. ACM, 2017.
- [8] Christian Szegedy, Wojciech Zaremba, Ilya Sutskever, Joan Bruna, Dumitru Erhan, Ian Goodfellow, and Rob Fergus. Intriguing properties of neural networks. *arXiv preprint arXiv:1312.6199*, 2013.
- [9] A. Nguyen, J. Yosinski, and J. Clune. Deep neural networks are easily fooled: High confidence predictions for unrecognizable images. In *2015 IEEE Conference on Computer Vision and Pattern Recognition (CVPR)*, pages 427–436, June 2015.

- [10] Ivan Evtimov, Kevin Eykholt, Earleence Fernandes, Tadayoshi Kohno, Bo Li, Atul Prakash, Amir Rahmati, and Dawn Song. Robust physical-world attacks on machine learning models. *arXiv preprint arXiv:1707.08945*, 2017.
- [11] Anish Athalye and Ilya Sutskever. Synthesizing robust adversarial examples. *arXiv preprint arXiv:1707.07397*, 2017.
- [12] Florian Tramèr, Alexey Kurakin, Nicolas Papernot, Dan Boneh, and Patrick McDaniel. Ensemble adversarial training: Attacks and defenses. *arXiv preprint arXiv:1705.07204*, 2017.
- [13] Nicolas Papernot, Patrick McDaniel, Xi Wu, Somesh Jha, and Ananthram Swami. Distillation as a defense to adversarial perturbations against deep neural networks. In *Security and Privacy (SP), 2016 IEEE Symposium on*, pages 582–597. IEEE, 2016.
- [14] Thilo Strauss, Markus Hanselmann, Andrej Junginger, and Holger Ulmer. Ensemble methods as a defense to adversarial perturbations against deep neural networks. *arXiv preprint arXiv:1709.03423*, 2017.
- [15] Shixiang Gu and Luca Rigazio. Towards deep neural network architectures robust to adversarial examples. *arXiv preprint arXiv:1412.5068*, 2014.
- [16] Alex Lamb, Jonathan Binas, Anirudh Goyal, Dmitriy Serdyuk, Sandeep Subramanian, Ioannis Mitliagkas, and Yoshua Bengio. Fortified networks: Improving the robustness of deep networks by modeling the manifold of hidden representations. *arXiv preprint arXiv:1804.02485*, 2018.
- [17] Aleksander Madry, Aleksandar Makelov, Ludwig Schmidt, Dimitris Tsipras, and Adrian Vladu. Towards deep learning models resistant to adversarial attacks. *arXiv preprint arXiv:1706.06083*, 2017.
- [18] Harini Kannan, Alexey Kurakin, and Ian Goodfellow. Adversarial logit pairing. *arXiv preprint arXiv:1803.06373*, 2018.
- [19] Xuanqing Liu, Yao Li, Chongruo Wu, and Cho-Jui Hsieh. Adv-bnn: Improved adversarial defense through robust bayesian neural network. *arXiv preprint arXiv:1810.01279*, 2018.
- [20] Cihang Xie, Yuxin Wu, Laurens van der Maaten, Alan Yuille, and Kaiming He. Feature denoising for improving adversarial robustness. *arXiv preprint arXiv:1812.03411*, 2018.
- [21] Lukas Schott, Jonas Rauber, Wieland Brendel, and Matthias Bethge. Robust perception through analysis by synthesis. *arXiv preprint arXiv:1805.09190*, 2018.
- [22] Yang Song, Taesup Kim, Sebastian Nowozin, Stefano Ermon, and Nate Kushman. Pixeldefend: Leveraging generative models to understand and defend against adversarial examples. *arXiv preprint arXiv:1710.10766*, 2017.
- [23] Pouya Samangouei, Maya Kabkab, and Rama Chellappa. Defense-gan: Protecting classifiers against adversarial attacks using generative models. *arXiv preprint arXiv:1805.06605*, 2018.
- [24] Andrew Ilyas, Ajil Jalal, Eirini Asteri, Constantinos Daskalakis, and Alexandros G Dimakis. The robust manifold defense: Adversarial training using generative models. *arXiv preprint arXiv:1712.09196*, 2017.
- [25] Shiwei Shen, Guoqing Jin, Ke Gao, and Yongdong Zhang. Ape-gan: Adversarial perturbation elimination with gan. *ICLR Submission, available on OpenReview*, 2017.
- [26] Chuan Guo, Mayank Rana, Moustapha Cissé, and Laurens van der Maaten. Countering adversarial images using input transformations. *arXiv preprint arXiv:1711.00117*, 2017.
- [27] Fangzhou Liao, Ming Liang, Yinpeng Dong, Tianyu Pang, Jun Zhu, and Xiaolin Hu. Defense against adversarial attacks using high-level representation guided denoiser. *arXiv preprint arXiv:1712.02976*, 2017.
- [28] Dongyu Meng and Hao Chen. Magnet: a two-pronged defense against adversarial examples. In *Proceedings of the 2017 ACM SIGSAC Conference on Computer and Communications Security*, pages 135–147. ACM, 2017.

- [29] Cihang Xie, Jianyu Wang, Zhishuai Zhang, Zhou Ren, and Alan Yuille. Mitigating adversarial effects through randomization. *arXiv preprint arXiv:1711.01991*, 2017.
- [30] Eric Wong and J Zico Kolter. Provable defenses against adversarial examples via the convex outer adversarial polytope. *arXiv preprint arXiv:1711.00851*, 2017.
- [31] Eric Wong, Frank Schmidt, Jan Hendrik Metzen, and J Zico Kolter. Scaling provable adversarial defenses. In *Advances in Neural Information Processing Systems*, pages 8400–8409, 2018.
- [32] Aditi Raghunathan, Jacob Steinhardt, and Percy Liang. Certified defenses against adversarial examples. *arXiv preprint arXiv:1801.09344*, 2018.
- [33] Krishnamurthy Dvijotham, Robert Stanforth, Sven Gowal, Timothy Mann, and Pushmeet Kohli. A dual approach to scalable verification of deep networks. *arXiv preprint arXiv:1803.06567*, 2018.
- [34] Gareth O Roberts and Jeffrey S Rosenthal. Optimal scaling of discrete approximations to langevin diffusions. *Journal of the Royal Statistical Society: Series B (Statistical Methodology)*, 60(1):255–268, 1998.
- [35] Gareth O Roberts, Richard L Tweedie, et al. Exponential convergence of langevin distributions and their discrete approximations. *Bernoulli*, 2(4):341–363, 1996.
- [36] Logan Engstrom, Andrew Ilyas, and Anish Athalye. Evaluating and understanding the robustness of adversarial logit pairing. *arXiv preprint arXiv:1807.10272*, 2018.
- [37] Anish Athalye, Nicholas Carlini, and David Wagner. Obfuscated gradients give a false sense of security: Circumventing defenses to adversarial examples. *arXiv preprint arXiv:1802.00420*, 2018.
- [38] Jonathan Uesato, Brendan O’Donoghue, Aaron van den Oord, and Pushmeet Kohli. Adversarial risk and the dangers of evaluating against weak attacks. *arXiv preprint arXiv:1802.05666*, 2018.
- [39] Nicholas Carlini, Anish Athalye, Nicolas Papernot, Wieland Brendel, Jonas Rauber, Dimitris Tsipras, Ian Goodfellow, and Aleksander Madry. On evaluating adversarial robustness. *arXiv preprint arXiv:1902.06705*, 2019.
- [40] Yinpeng Dong, Fangzhou Liao, Tianyu Pang, Hang Su, Jun Zhu, Xiaolin Hu, and Jianguo Li. Boosting adversarial attacks with momentum. *arXiv preprint*, 2018.
- [41] Nicholas Carlini and David Wagner. Towards evaluating the robustness of neural networks. In *Security and Privacy (SP), 2017 IEEE Symposium on*, pages 39–57. IEEE, 2017.
- [42] Pin-Yu Chen, Yash Sharma, Huan Zhang, Jinfeng Yi, and Cho-Jui Hsieh. Ead: elastic-net attacks to deep neural networks via adversarial examples. *arXiv preprint arXiv:1709.04114*, 2017.
- [43] Yash Sharma and Pin-Yu Chen. Breaking the madry defense model with l_1 -based adversarial examples. *arXiv preprint arXiv:1710.10733*, 2017.
- [44] Nicholas Frosst, Sara Sabour, and Geoffrey Hinton. Darccc: Detecting adversaries by reconstruction from class conditional capsules. *arXiv preprint arXiv:1811.06969*, 2018.
- [45] Nicolas Papernot, Patrick McDaniel, and Ian Goodfellow. Transferability in machine learning: from phenomena to black-box attacks using adversarial samples. *arXiv preprint arXiv:1605.07277*, 2016.
- [46] Wieland Brendel, Jonas Rauber, and Matthias Bethge. Decision-based adversarial attacks: Reliable attacks against black-box machine learning models. *arXiv preprint arXiv:1712.04248*, 2017.
- [47] Dan Hendrycks and Thomas G Dietterich. Benchmarking neural network robustness to common corruptions and surface variations. *arXiv preprint arXiv:1807.01697*, 2018.
- [48] Florian Tramèr, Nicolas Papernot, Ian Goodfellow, Dan Boneh, and Patrick McDaniel. The space of transferable adversarial examples. *arXiv preprint arXiv:1704.03453*, 2017.
- [49] Alexey Kurakin, Ian Goodfellow, and Samy Bengio. Adversarial machine learning at scale. *arXiv preprint arXiv:1611.01236*, 2016.

- [50] Chuan Guo, Mayank Rana, Moustapha Cisse, and Laurens van der Maaten. Countering adversarial images using input transformations. *arXiv preprint arXiv:1711.00117*, 2017.
- [51] Nicholas Carlini and David Wagner. Magnet and "efficient defenses against adversarial attacks" are not robust to adversarial examples. *arXiv preprint arXiv:1711.08478*, 2017.
- [52] Aman Sinha, Hongseok Namkoong, and John Duchi. Certifying some distributional robustness with principled adversarial training. *arXiv preprint arXiv:1710.10571*, 2017.
- [53] Anh Nguyen, Jason Yosinski, Yoshua Bengio, Alexey Dosovitskiy, and Jeff Clune. Plug & play generative networks: Conditional iterative generation of images in latent space. *arXiv preprint arXiv:1612.00005*, 2016.
- [54] Pascal Vincent, Hugo Larochelle, Yoshua Bengio, and Pierre-Antoine Manzagol. Extracting and composing robust features with denoising autoencoders. In *Proceedings of the 25th international conference on Machine learning*, pages 1096–1103. ACM, 2008.
- [55] Guillaume Alain and Yoshua Bengio. What regularized auto-encoders learn from the data-generating distribution. *The Journal of Machine Learning Research*, 15(1):3563–3593, 2014.
- [56] Unknown. Learning by denoising part 2. connection between data distribution and denoising function, 2016.
- [57] Seyed-Mohsen Moosavi-Dezfooli, Alhussein Fawzi, and Pascal Frossard. Deepfool: a simple and accurate method to fool deep neural networks. In *Proceedings of the IEEE Conference on Computer Vision and Pattern Recognition*, pages 2574–2582, 2016.
- [58] Andrew Ilyas, Logan Engstrom, Anish Athalye, and Jessy Lin. Query-efficient black-box adversarial examples. *arXiv preprint arXiv:1712.07113*, 2017.
- [59] Pu Zhao, Sijia Liu, Yanzhi Wang, and Xue Lin. An admn-based universal framework for adversarial attacks on deep neural networks. *arXiv preprint arXiv:1804.03193*, 2018.
- [60] Grégoire Montavon, Wojciech Samek, and Klaus-Robert Müller. Methods for interpreting and understanding deep neural networks. *Digital Signal Processing*, 73:1–15, 2018.
- [61] Sebastian Lapuschkin, Stephan Wäldchen, Alexander Binder, Grégoire Montavon, Wojciech Samek, and Klaus-Robert Müller. Unmasking clever hans predictors and assessing what machines really learn. *Nature communications*, 10(1):1096, 2019.
- [62] H Brendan McMahan, Eider Moore, Daniel Ramage, Seth Hampson, et al. Communication-efficient learning of deep networks from decentralized data. *arXiv preprint arXiv:1602.05629*, 2016.
- [63] Felix Sattler, Simon Wiedemann, Klaus-Robert Müller, and Wojciech Samek. Sparse binary compression: Towards distributed deep learning with minimal communication. *arXiv:1805.08768*, 2018.
- [64] Martín Abadi, Paul Barham, Jianmin Chen, Zhifeng Chen, Andy Davis, Jeffrey Dean, Matthieu Devin, Sanjay Ghemawat, Geoffrey Irving, Michael Isard, et al. Tensorflow: a system for large-scale machine learning. In *OSDI*, volume 16, pages 265–283, 2016.
- [65] Mark Girolami and Ben Calderhead. Riemann manifold langevin and hamiltonian monte carlo methods. *Journal of the Royal Statistical Society: Series B (Statistical Methodology)*, 73(2):123–214, 2011.

A Proof of Theorem 1

sDAE is trained so that the following functional is minimized with respect to the function $\mathbf{r} : \mathbb{R}^L \mapsto \mathbb{R}^L$:

$$g(\mathbf{r}) = \mathbb{E}_{p'(\mathbf{x}, \mathbf{y})p'(\boldsymbol{\nu})} [\|\mathbf{r}(\mathbf{x} + \boldsymbol{\nu}) - \mathbf{x}\|^2 - 2\sigma^2 J(\mathbf{r}(\mathbf{x} + \boldsymbol{\nu}), \mathbf{y})], \quad (13)$$

which is a finite sample approximation to the true objective

$$g(\mathbf{r}) = \int (\|\mathbf{r}(\mathbf{x} + \boldsymbol{\nu}) - \mathbf{x}\|^2 - 2\sigma^2 \mathbb{E}_{p(\mathbf{y}|\mathbf{x})} [\log p(\mathbf{y}|\mathbf{r}(\mathbf{x} + \boldsymbol{\nu}))]) p(\mathbf{x}) \mathcal{N}_L(\boldsymbol{\nu}; \mathbf{0}, \sigma^2 \mathbf{I}) d\mathbf{x} d\boldsymbol{\nu}. \quad (14)$$

We assume that $\mathbf{r}(\mathbf{x})$ and $p(\mathbf{y}|\mathbf{x})$ are analytic functions with respect to \mathbf{x} . For small σ^2 , the Taylor expansion of the l -th component of \mathbf{r} around \mathbf{x} gives

$$r_l(\mathbf{x} + \boldsymbol{\nu}) = r_l(\mathbf{x}) + \boldsymbol{\nu}^\top \frac{\partial r_l}{\partial \mathbf{x}} + \frac{1}{2} \boldsymbol{\nu}^\top \frac{\partial^2 r_l}{\partial \mathbf{x} \partial \mathbf{x}} \boldsymbol{\nu} + O(\sigma^3),$$

where $\frac{\partial^2 f}{\partial \mathbf{x} \partial \mathbf{x}}$ is the Hessian of a function $f(\mathbf{x})$. Substituting this into Eq.(14), we have

$$\begin{aligned} g &= \int \left\{ \sum_{l=1}^L \left(r_l(\mathbf{x}) + \boldsymbol{\nu}^\top \frac{\partial r_l}{\partial \mathbf{x}} + \frac{1}{2} \boldsymbol{\nu}^\top \frac{\partial^2 r_l}{\partial \mathbf{x} \partial \mathbf{x}} \boldsymbol{\nu} - x_l \right)^2 \right. \\ &\quad \left. - 2\sigma^2 \mathbb{E}_{p(\mathbf{y}|\mathbf{x})} [\log p(\mathbf{y}|\mathbf{r}(\mathbf{x}))] \right\} p(\mathbf{x}) d\mathbf{x} \mathcal{N}_L(\boldsymbol{\nu}; \mathbf{0}, \sigma^2 \mathbf{I}) d\boldsymbol{\nu} + O(\sigma^3) \\ &= \int \left\{ \sum_{l=1}^L \left((r_l(\mathbf{x}) - x_l)^2 + (r_l(\mathbf{x}) - x_l) \boldsymbol{\nu}^\top \frac{\partial^2 r_l}{\partial \mathbf{x} \partial \mathbf{x}} \boldsymbol{\nu} + \frac{\partial r_l}{\partial \mathbf{x}}^\top \boldsymbol{\nu} \boldsymbol{\nu}^\top \frac{\partial r_l}{\partial \mathbf{x}} \right) \right. \\ &\quad \left. - 2\sigma^2 \mathbb{E}_{p(\mathbf{y}|\mathbf{x})} [\log p(\mathbf{y}|\mathbf{r}(\mathbf{x}))] \right\} p(\mathbf{x}) d\mathbf{x} \mathcal{N}_L(\boldsymbol{\nu}; \mathbf{0}, \sigma^2 \mathbf{I}) d\boldsymbol{\nu} + O(\sigma^3) \\ &= \int \left\{ \sum_{l=1}^L \left((r_l(\mathbf{x}) - x_l)^2 + \sigma^2 (r_l(\mathbf{x}) - x_l) \text{tr} \left(\frac{\partial^2 r_l}{\partial \mathbf{x} \partial \mathbf{x}} \right) + \sigma^2 \left\| \frac{\partial r_l}{\partial \mathbf{x}} \right\|^2 \right) \right. \\ &\quad \left. - 2\sigma^2 \mathbb{E}_{p(\mathbf{y}|\mathbf{x})} [\log p(\mathbf{y}|\mathbf{r}(\mathbf{x}))] \right\} p(\mathbf{x}) d\mathbf{x} + O(\sigma^3). \end{aligned} \quad (15)$$

Thus, the objective functional (14) can be written as

$$g(\mathbf{r}) = \int G d\mathbf{x} + O(\sigma^3), \quad (16)$$

where

$$\begin{aligned} G &= \left\{ \sum_{l=1}^L \left((r_l(\mathbf{x}) - x_l + \sigma^2 \text{tr} \left(\frac{\partial^2 r_l}{\partial \mathbf{x} \partial \mathbf{x}} \right)) (r_l(\mathbf{x}) - x_l) + \sigma^2 \left\| \frac{\partial r_l}{\partial \mathbf{x}} \right\|^2 \right) \right. \\ &\quad \left. - 2\sigma^2 \mathbb{E}_{p(\mathbf{y}|\mathbf{x})} [\log p(\mathbf{y}|\mathbf{r}(\mathbf{x}))] \right\} p(\mathbf{x}). \end{aligned} \quad (17)$$

We can find the optimal function minimizing the functional (16) by using *calculus of variations*. The optimal function satisfies the following Euler-Lagrange equation: for each $l = 1, \dots, L$,

$$\frac{\partial G}{\partial r_l} - \sum_{m=1}^L \frac{\partial}{\partial x_m} \frac{\partial G}{\partial (r'_l)_m} + \sum_{m=1}^L \sum_{m'=m+1}^L \frac{\partial^2}{\partial x_m \partial x_{m'}} \frac{\partial G}{\partial (\mathbf{R}''_l)_{m,m'}} = 0, \quad (18)$$

where $\mathbf{r}'_l = \frac{\partial r_l}{\partial \mathbf{x}} \in \mathbb{R}^L$ is the gradient (of r_l with respect to \mathbf{x}) and $\mathbf{R}''_l = \frac{\partial^2 r_l}{\partial \mathbf{x} \partial \mathbf{x}} \in \mathbb{R}^{L \times L}$ is the Hessian.

We have

$$\begin{aligned} \frac{\partial G}{\partial r_l} &= \left\{ 2(r_l(\mathbf{x}) - x_l) + \sigma^2 \text{tr} \left(\frac{\partial^2 r_l}{\partial \mathbf{x} \partial \mathbf{x}} \right) - 2\sigma^2 \frac{\partial \mathbb{E}_{p(\mathbf{y}|\mathbf{x})} [\log p(\mathbf{y}|\mathbf{r}(\mathbf{x}))]}{\partial r_l} \right\} p(\mathbf{x}), \\ \frac{\partial G}{\partial (r'_l)_m} &= 2\sigma^2 \frac{\partial r_l}{\partial x_m} p(\mathbf{x}), \\ \frac{\partial G}{\partial (\mathbf{R}''_l)_{m,m'}} &= \delta_{m,m'} \sigma^2 (r_l(\mathbf{x}) - x_l) p(\mathbf{x}), \end{aligned}$$

and therefore

$$\begin{aligned}\frac{\partial}{\partial x_m} \frac{\partial G}{\partial (\mathbf{r}'_l)_m} &= 2\sigma^2 \left(\frac{\partial^2 r_l}{\partial x_m^2} p(\mathbf{x}) + \frac{\partial r_l}{\partial x_m} \frac{\partial p(\mathbf{x})}{\partial x_m} \right), \\ \frac{\partial^2}{\partial x_m \partial x_{m'}} \frac{\partial G}{\partial (\mathbf{R}''_l)_{m,m'}} &= \sigma^2 \delta_{m,m'} \frac{\partial}{\partial x_m} \left(\left(\frac{\partial r_l}{\partial x_{m'}} - \delta_{l,m'} \right) p(\mathbf{x}) + (r_l(\mathbf{x}) - x_l) \frac{\partial p(\mathbf{x})}{\partial x_{m'}} \right) \\ &= \sigma^2 \delta_{m,m'} \left(\frac{\partial^2 r_l}{\partial x_m^2} p(\mathbf{x}) + 2 \left(\frac{\partial r_l}{\partial x_m} - \delta_{l,m} \right) \frac{\partial p(\mathbf{x})}{\partial x_m} + (r_l(\mathbf{x}) - x_l) \frac{\partial^2 p(\mathbf{x})}{\partial x_m^2} \right),\end{aligned}$$

where $\delta_{m,m'}$ is the Kronecker delta. Substituting the above into Eq.(18), we have

$$\begin{aligned}& \left\{ 2(r_l(\mathbf{x}) - x_l) + \sigma^2 \text{tr} \left(\frac{\partial^2 r_l}{\partial \mathbf{x} \partial \mathbf{x}} \right) - 2\sigma^2 \frac{\partial \mathbb{E}_{p(\mathbf{y}|\mathbf{x})} [\log p(\mathbf{y}|\mathbf{r}(\mathbf{x}))]}{\partial r_l} \right\} p(\mathbf{x}) \\ & + \sigma^2 \sum_{m=1}^L \sum_{m'=m+1}^L \delta_{m,m'} \left(\frac{\partial^2 r_l}{\partial x_m^2} p(\mathbf{x}) + 2 \left(\frac{\partial r_l}{\partial x_m} - \delta_{l,m} \right) \frac{\partial p(\mathbf{x})}{\partial x_m} + (r_l(\mathbf{x}) - x_l) \frac{\partial^2 p(\mathbf{x})}{\partial x_m^2} \right) \\ & - 2\sigma^2 \sum_{m=1}^L \left(\frac{\partial^2 r_l}{\partial x_m^2} p(\mathbf{x}) + \frac{\partial r_l}{\partial x_m} \frac{\partial p(\mathbf{x})}{\partial x_m} \right) = 0,\end{aligned}\tag{19}$$

and therefore

$$\left(r_l(\mathbf{x}) - x_l - \sigma^2 \frac{\partial \mathbb{E}_{p(\mathbf{y}|\mathbf{x})} [\log p(\mathbf{y}|\mathbf{r}(\mathbf{x}))]}{\partial r_l} \right) \left(1 + \frac{\sigma^2}{2p(\mathbf{x})} \text{tr} \left(\frac{\partial^2 p(\mathbf{x})}{\partial \mathbf{x} \partial \mathbf{x}} \right) \right) - \sigma^2 \frac{1}{p(\mathbf{x})} \frac{\partial p(\mathbf{x})}{\partial x_l} = 0.$$

Since

$$\begin{aligned}\frac{\partial \log p(\mathbf{x})}{\partial x_m} &= \frac{1}{p(\mathbf{x})} \frac{\partial p(\mathbf{x})}{\partial x_m}, \\ \frac{\partial^2 \log p(\mathbf{x})}{\partial x_m \partial x_{m'}} &= \frac{\partial}{\partial x_{m'}} \left(\frac{1}{p(\mathbf{x})} \frac{\partial p(\mathbf{x})}{\partial x_m} \right) \\ &= -\frac{\partial \log p(\mathbf{x})}{\partial x_{m'}} \frac{\partial \log p(\mathbf{x})}{\partial x_m} + \frac{1}{p(\mathbf{x})} \frac{\partial^2 p(\mathbf{x})}{\partial x_m \partial x_{m'}}, \\ \frac{\partial \mathbb{E}_{p(\mathbf{y}|\mathbf{x})} [\log p(\mathbf{y}|\mathbf{r}(\mathbf{x}))]}{\partial r_l} &= \mathbb{E}_{p(\mathbf{y}|\mathbf{x})} \left[\frac{\partial \log p(\mathbf{y}|\mathbf{x})}{\partial x_l} \Big|_{\mathbf{x}=\mathbf{r}(\mathbf{x})} \right],\end{aligned}$$

we have

$$\begin{aligned}& \left(r_l(\mathbf{x}) - x_l - \sigma^2 \mathbb{E}_{p(\mathbf{y}|\mathbf{x})} \left[\frac{\partial \log p(\mathbf{y}|\mathbf{x})}{\partial x_l} \Big|_{\mathbf{x}=\mathbf{r}(\mathbf{x})} \right] \right) \left(1 + \frac{\sigma^2}{2} \left(\text{tr} \left(\frac{\partial^2 \log p(\mathbf{x})}{\partial \mathbf{x} \partial \mathbf{x}} \right) + \left\| \frac{\partial \log p(\mathbf{x})}{\partial \mathbf{x}} \right\|^2 \right) \right) \\ & - \sigma^2 \frac{\partial \log p(\mathbf{x})}{\partial x_l} = 0,\end{aligned}$$

and therefore

$$\begin{aligned}r_l(\mathbf{x}) - x_l &= \sigma^2 \mathbb{E}_{p(\mathbf{y}|\mathbf{x})} \left[\frac{\partial \log p(\mathbf{y}|\mathbf{x})}{\partial x_l} \Big|_{\mathbf{x}=\mathbf{r}(\mathbf{x})} \right] \\ & + \sigma^2 \frac{\partial \log p(\mathbf{x})}{\partial x_l} \left(1 + \frac{\sigma^2}{2} \left(\text{tr} \left(\frac{\partial^2 \log p(\mathbf{x})}{\partial \mathbf{x} \partial \mathbf{x}} \right) + \left\| \frac{\partial \log p(\mathbf{x})}{\partial \mathbf{x}} \right\|^2 \right) \right)^{-1} \\ & = \sigma^2 \mathbb{E}_{p(\mathbf{y}|\mathbf{x})} \left[\frac{\partial \log p(\mathbf{y}|\mathbf{x})}{\partial x_l} \Big|_{\mathbf{x}=\mathbf{r}(\mathbf{x})} \right] + \sigma^2 \frac{\partial \log p(\mathbf{x})}{\partial x_l} + O(\sigma^4).\end{aligned}$$

Taking the asymptotic term in Eq.(16) into account, we have

$$r_l(\mathbf{x}) - x_l = \sigma^2 \mathbb{E}_{p(\mathbf{y}|\mathbf{x})} \left[\frac{\partial \log p(\mathbf{y}|\mathbf{x})}{\partial x_l} \Big|_{\mathbf{x}=\mathbf{r}(\mathbf{x})} \right] + \sigma^2 \frac{\partial \log p(\mathbf{x})}{\partial x_l} + O(\sigma^3),$$

which implies that $\mathbf{r}(\mathbf{x}) = \mathbf{x} + O(\sigma^2)$. Thus, we conclude that

$$\begin{aligned}r_l(\mathbf{x}) - x_l &= \sigma^2 \mathbb{E}_{p(\mathbf{y}|\mathbf{x})} \left[\frac{\partial \log p(\mathbf{y}|\mathbf{x})}{\partial x_l} \right] + \sigma^2 \frac{\partial \log p(\mathbf{x})}{\partial x_l} + O(\sigma^3), \\ &= \sigma^2 \mathbb{E}_{p(\mathbf{y}|\mathbf{x})} \left[\frac{\partial}{\partial x_l} \log p(\mathbf{x}, \mathbf{y}) \right] + O(\sigma^3),\end{aligned}\tag{20}$$

which completes the proof of Theorem 1.

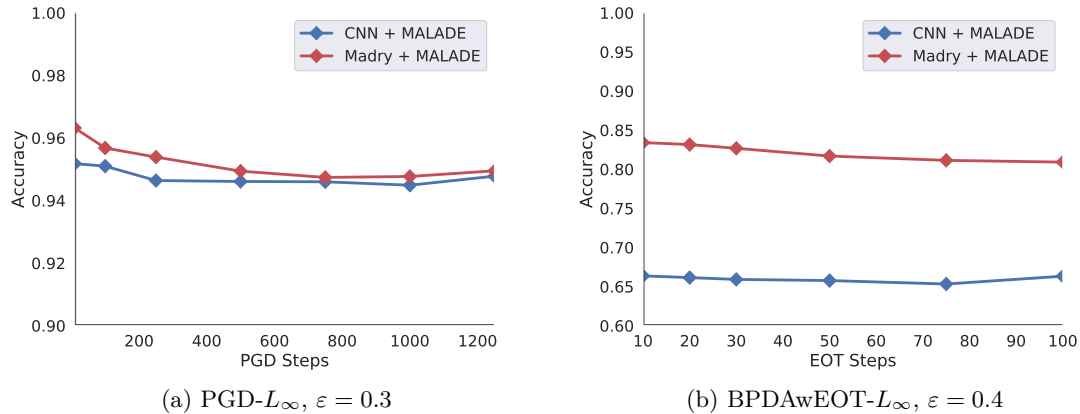


Figure 6: Accuracy is plotted against the number of iterations performed by the attacking method for fixed distortion.

B Implementation Details

We implemented our attacks using *cleverhans* repository ⁷, code of ALP [18]⁸ and also the code of Madry⁹. The code was written in Tensorflow [64]

B.1 Hyper-parameter Settings for the Attacks

B.1.1 PGD

PGD attack was an untargeted attack as it is the simplest strategy for attacking. Learning rate of 0.01 was found to provide for a strong attack while number of iterations was tested for different values as shown in Fig. 6a and fixed at $N = 1000$. Similar hyper-parameters were used for MIM attack.

B.1.2 BPDawEOT

The attack strategy against MALADE was tested for its effectiveness by varying the number of steps of EOT to be computed. As shown in Fig. 6b $N = 30$ was found to be sufficient for optimal convergence of the attack.

B.1.3 CW

Hyper-parameters tuned include learning rate = 0.1 and number of iterations $N = 1000$, initial constant $c = 100$, binary search step = 1 and confidence = 0. The optimizer used here was Adam optimizer.

B.1.4 EAD

Hyper-parameters tuned for attacking MALADE include learning rate = 0.01 and number of iterations $N = 100$, initial constant $c = 0.01$, binary search step = 9 and confidence = 0. Increasing the number of iterations did not show any increase in the strength of the attack. On the other hand, increasing the number of iterations proved useful for attacking [17], although with all the hyper-parameters being the same. The Adam optimizer was investigated for this attack as recommended by [42, 43], however Gradient Descent optimizer proved better in the convergence of the attack.

B.2 Score Function Estimation

B.2.1 Training sDAE

The score function $\nabla_{\mathbf{x}} \log p(\mathbf{x})$ provided by DAE is dependent on the noise σ^2 added to the input while training the DAE. While too small values for σ^2 make the score function highly unstable, too large values

⁷<https://github.com/tensorflow/cleverhans>

⁸https://github.com/tensorflow/models/tree/master/research/adversarial_logit_pairing

⁹https://github.com/MadryLab/mnist_challenge

blur the score. The same is true for the score function $\nabla_{\mathbf{x}} \log p(\mathbf{x}|\mathbf{y})$ provided by MALADE. Here in our experiments on MNIST, we trained the DAE as well as the sDAE with $\sigma^2 = 0.15$. Such a large noise is beneficial for reliable estimation of the score function [53]. On the other hand, for CIFAR10 and TinyImagenet datasets, due to the complexity of the dataset, we used $\sigma^2 = 0.01$.

B.2.2 Step Size for Malade

The score function provided by MALADE drives the generated sample towards high density regions in the data generating distributions. With the direction provided by the score function, α controls the distance to move agt each step. With large α , there is possibility of jumping out of the data manifold. While annealing α and δ^2 would provides best results as the samples move towards high density region [34, 65]. In our experiments, we train the sDAE (or DAE) first, followed by searching for good parameters for the α and number of steps on the training or validation set. This reasonable procedure allows for manually finetuning the step size and number of steps based on the difficulty of the dataset, such that they samples are driven to the nearest high density region of the correct label in polynomial time. In the case of adversarial robustness, it also important to select the hyperparameters such that the off-manifold adversarial examples are returned to the data manifold of the correct label in the given number of steps. These parameters are then fixed and evaluated on the test set for each of the datasets.

B.3 Model Architecture

B.3.1 Classifier and DAE (and sDAE) Architecture on MNIST

In this appendix, we summarize the architectures of the deep neural networks we used in all experiments. Table 5 gives the architectures of the classifier models while Table 6 gives the architecture of the DAE and sDAE models (both have the same architecture).

Conv represents convolution, with the format of Conv(number of output filter maps, kernel size, stride size). *Linear* represents a fully connected layer with the format of Linear(number of output neurons). *Relu* is a rectified linear unit while *Tanh* is a hyberbolic tangent function. *Softmax* is a logistic function which squashes the input tensor to real values of range [0,1] and adds up to 1. *Conv_Transpose* is transpose of the convolution operation, sometimes called deconvolution, with the format of Conv_Transpose(number of output filter maps, kernel size, stride size).

Table 5: Architectures of Classifier

CNN
Conv(128, 3 × 3, 1)
Relu()
Conv(64, 5 × 5, 2)
Relu()
Linear(128)
Relu()
Linear(10)
Softmax()

B.3.2 CIFAR10

The CNN architecture for CIFAR10 was borrowed from Tensorflow library¹⁰. The model of Madry for CIFAR10 dataset is as implemented by the authors in [17].

B.3.3 TinyImagenet

The architecture and the pretrained models of CNN as well as ALP is as implemented by the authors¹¹.

¹⁰<https://github.com/tensorflow/models/tree/master/official/resnet>

¹¹https://github.com/tensorflow/models/tree/master/research/adversarial_logit_pairing

Table 6: Architecture of DAE and sDAE.

DAE, sDAE	
Encoder	Conv(10, 5×5 , 2)
	Tanh()
	Conv(25, 5×5 , 2)
	Tanh()
Decoder	Conv_Transpose(10, 9×9 , 2)
	Tanh()
	Conv_Transpose(1, 1×1 , 2)
	Tanh()
	Conv(1, 5×5 , 1)
	Tanh()

C Effect of EOT

In order to eliminate random effect, and obtain useful gradient information for the attacker, we formulated BPDawEOT against Madry + MALADE and found this to be the strongest attack. Fig. 7 shows the adversarial perturbations of PGD on Madry + MALADE results in perturbations that appear to be blobs throughout the image. Adversarial images from BPDawEOT on the other hand are similar to the perturbations crafted by the attacker for PGD on Madry alone – indicating that the phenomenon of gradients obfuscation is prevented. Nevertheless, the adversarial samples against MALADE are not as effective as against Madry, as shown in Fig. 4. This is because the inherent randomness of MALADE prevents the attack from stably aligning the sample to a targeted untrained spot.

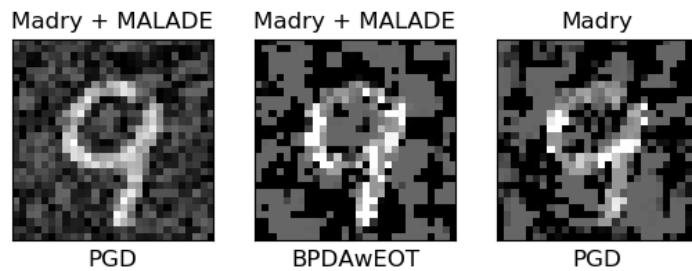


Figure 7: The adversarial examples shown here correspond to - PGD- L_∞ attack for Madry + MALADE, BPDawEOT for Madry + MALADE and finally PGD- L_∞ for Madry. The maximum perturbation allowed in all of these settings was $\varepsilon = 0.4$. The effect of gradient obfuscation is visible in the first image while BPDawEOT is effective in preventing this phenomenon.

D Adversarial Samples

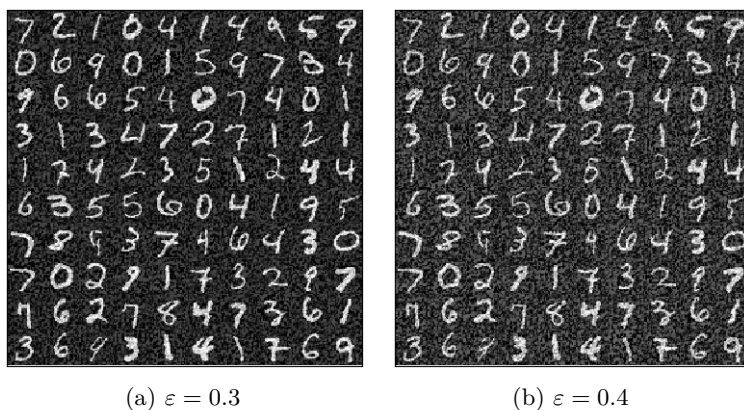


Figure 8: Sample adversarial images crafted by a PGD attack with L_∞ norm are shown here.

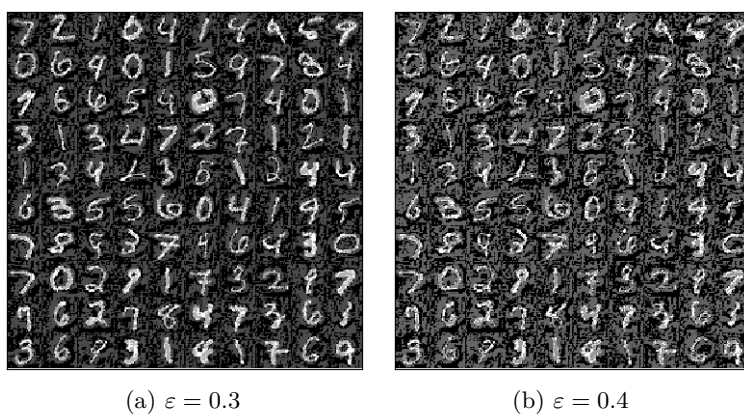


Figure 9: Sample adversarial images crafted by R+PGD attack with L_∞ norm are shown here.

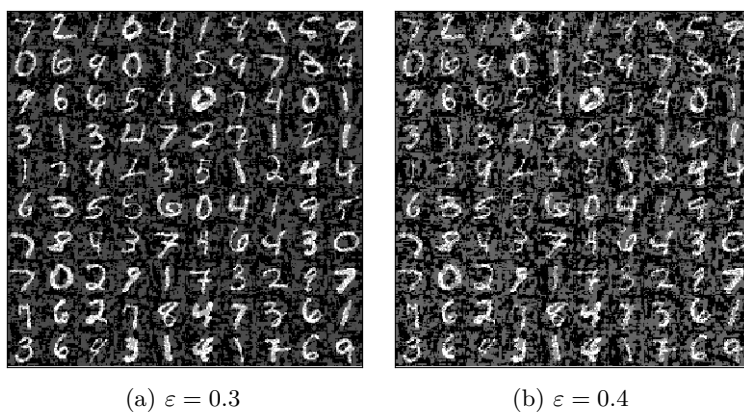


Figure 10: Sample adversarial images crafted by a BPDA attack with L_∞ norm are shown here.

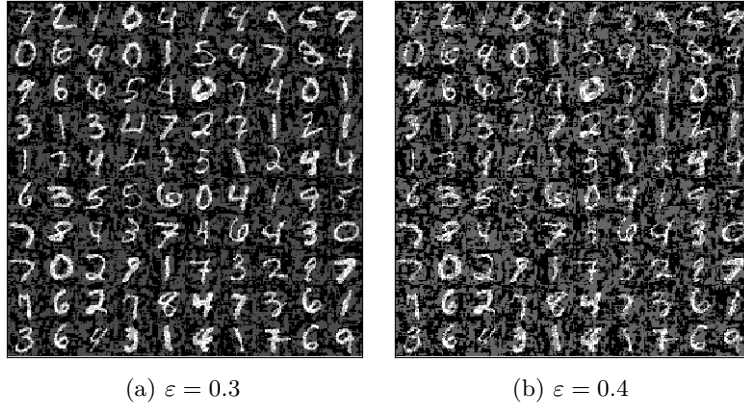


Figure 11: Sample adversarial images crafted by a BPDawEOT attack with L_∞ norm are shown here.

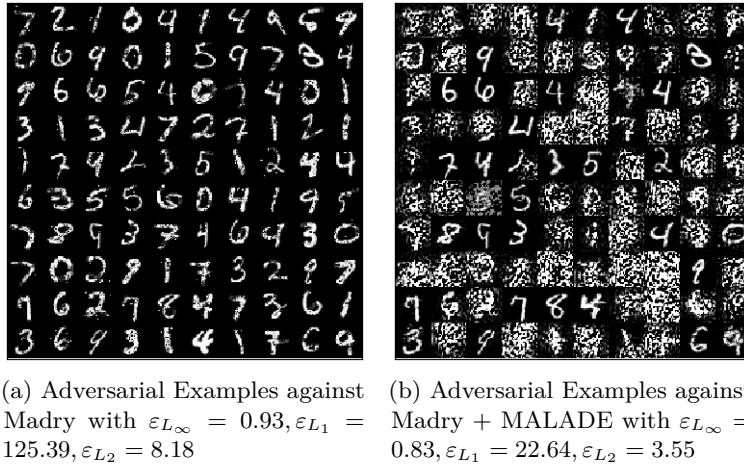


Figure 12: Sample adversarial images crafted by EAD attack are shown here. The attack fails to converge for many images despite our best effort to finetune the algorithm.

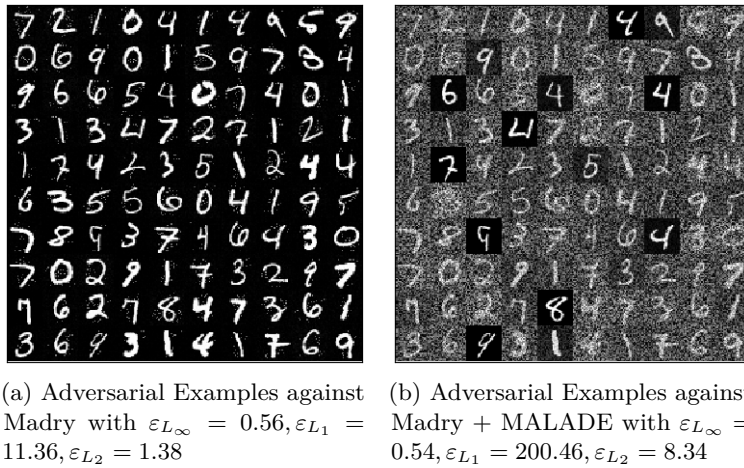
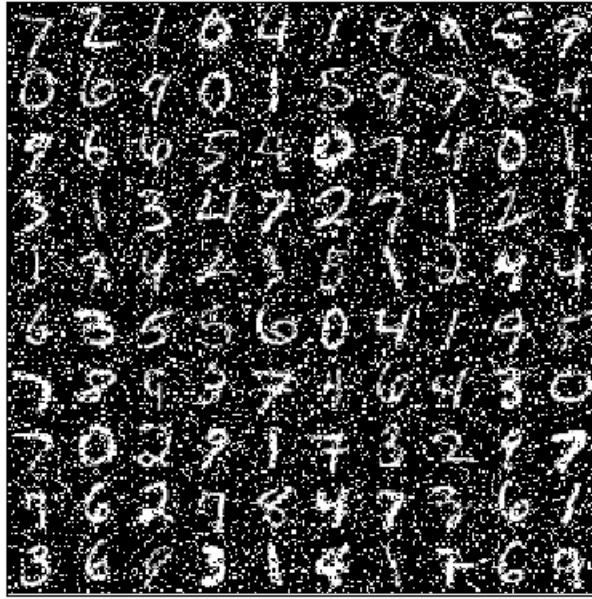
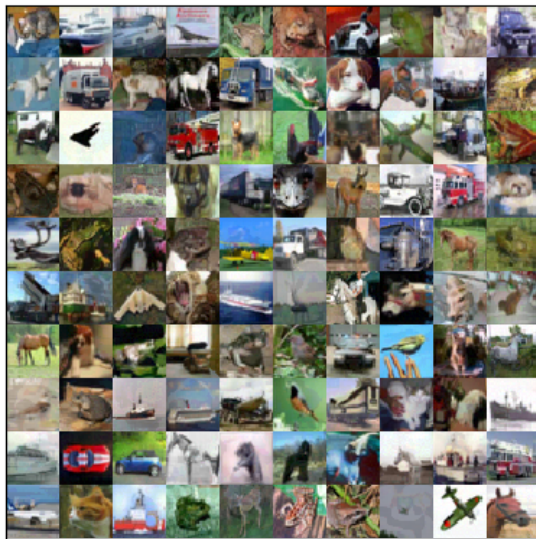


Figure 13: Sample adversarial images crafted by a Boundary attack are shown here. Some images fail to become adversarial during the initialization of the algorithm with random uniform noise and hence are retained as the original image.



(a) Images corrupted by Salt and Pepper Noise Attack with $\varepsilon_{L_\infty} = 0.99, \varepsilon_{L_1} = 98.02, \varepsilon_{L_2} = 9.70$

Figure 14: Sample adversarial images crafted by adding salt and pepper noise are shown here. The mean of the magnitude of the perturbations over the entire test dataset for each distance measure is given below each image.

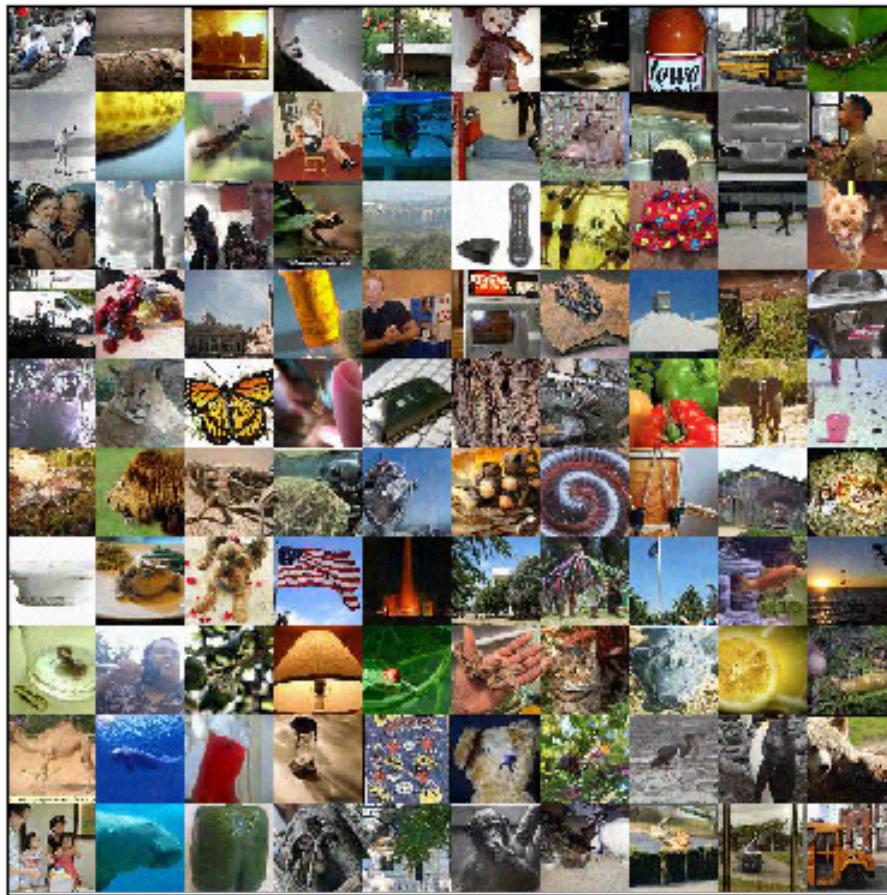


(a) $\varepsilon = 8.0$

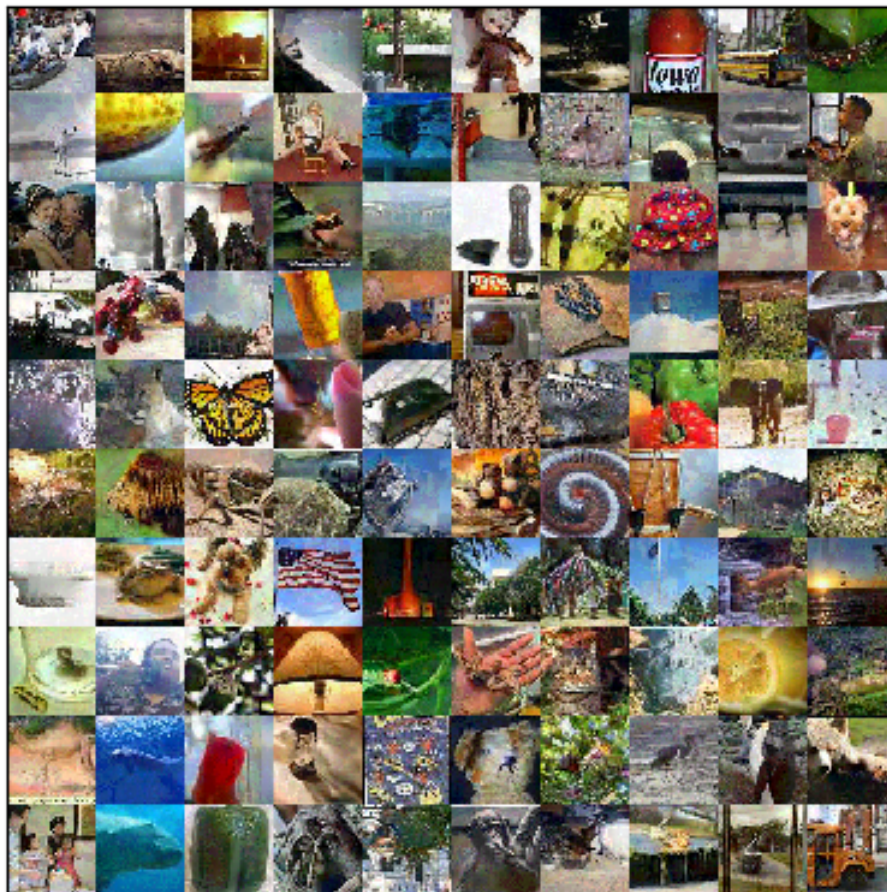


(b) $\varepsilon = 16.0$

Figure 15: Sample adversarial images crafted by PGD L_∞ attack against Madry + MALADE for the CIFAR10 dataset are shown here.

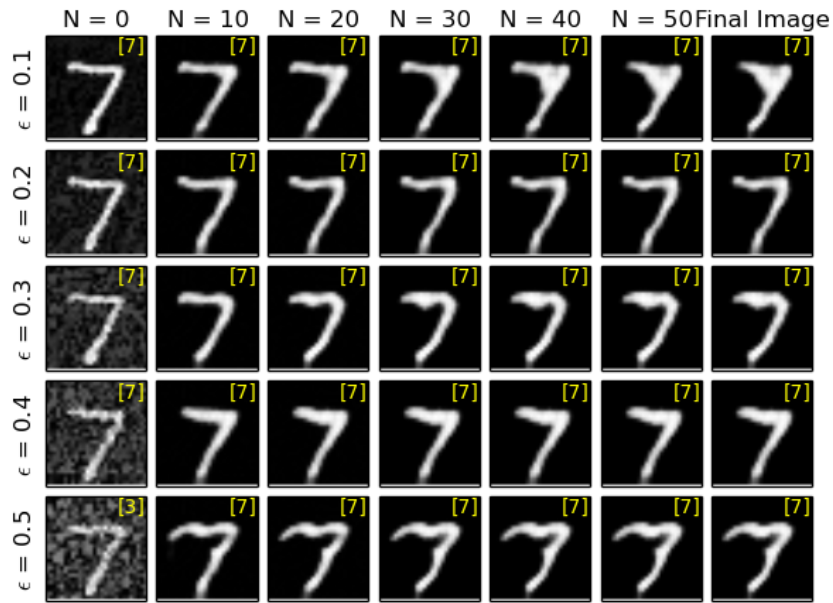


(a) $\varepsilon = 8.0$

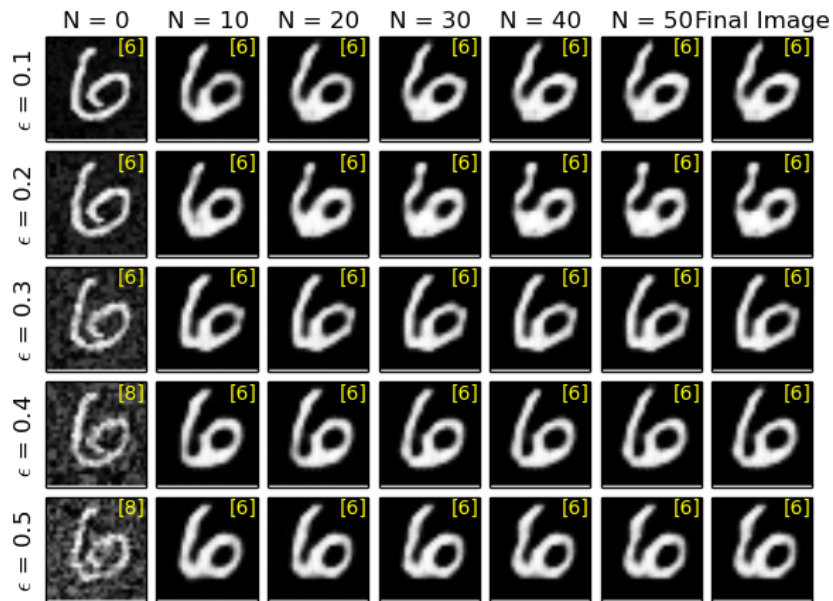


(b) $\varepsilon = \frac{16.0}{25}$

Figure 16: Sample adversarial images crafted by PGD L_∞ attack against ALP + MALADE for the TinyImageNet dataset are shown here.

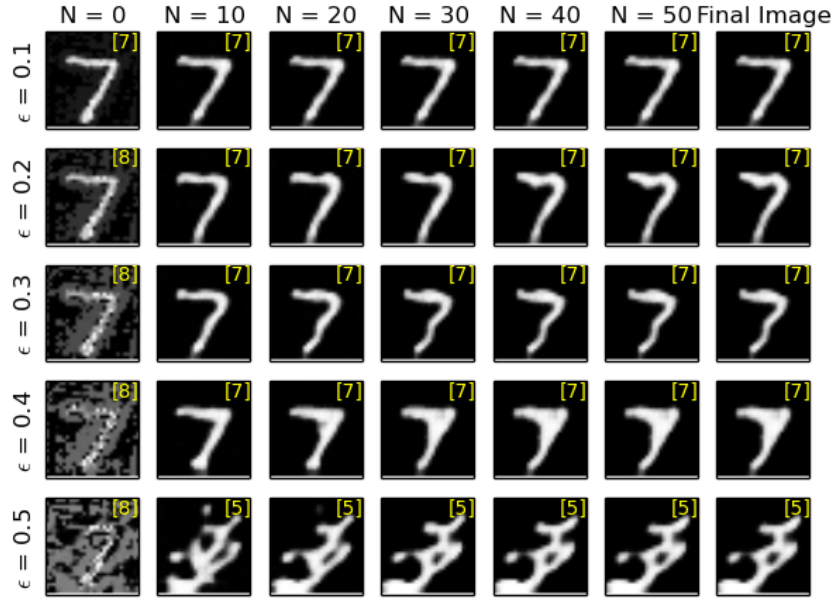


(a)

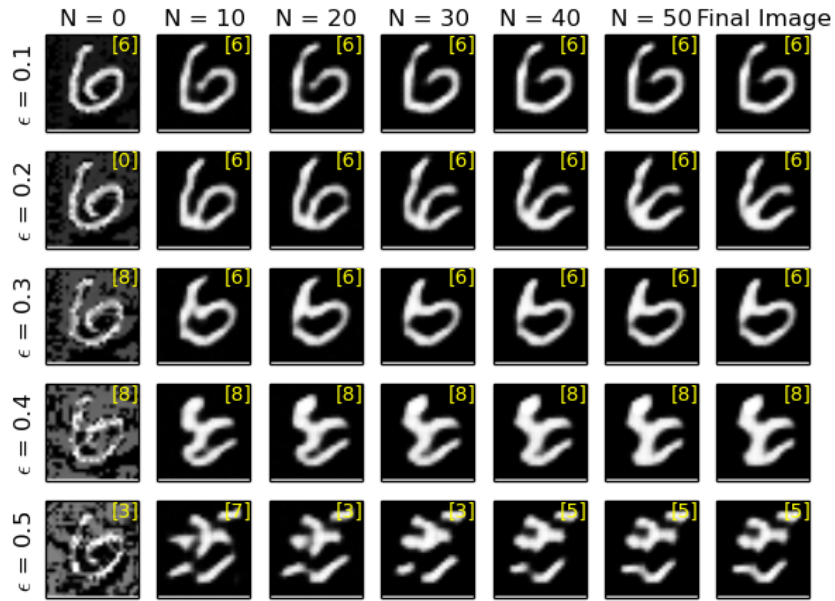


(b)

Figure 17: Sample images for the MALADE algorithm against a PGD attack with L_∞ norm are shown here. The rows indicate the norm of the perturbation used by the attacked while the columns indicate the intermittent steps taken by MALADE to defend the attack. The classifier’s decision is displayed in yellow in the top right corner of each image. Due to gradient obfuscation, the adversarial samples are not very strong and hence MALADE is very robust here.

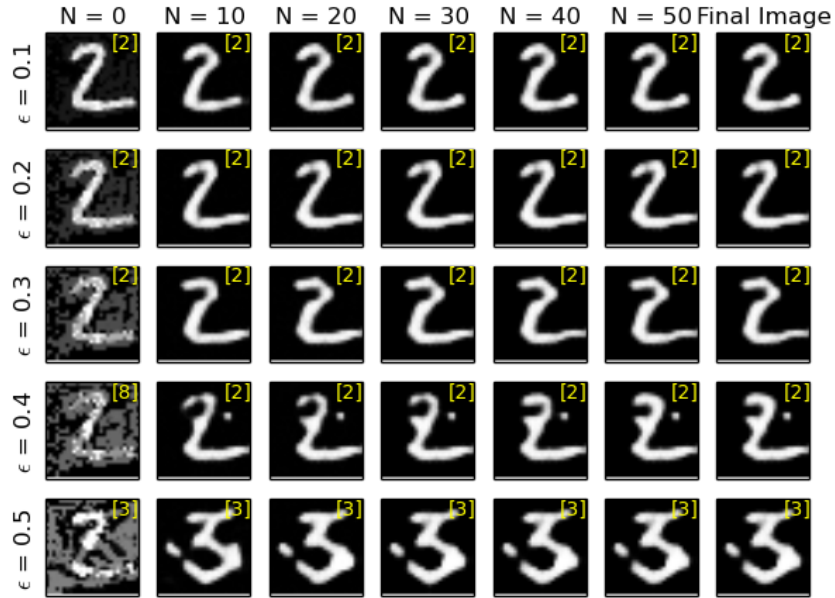


(a)

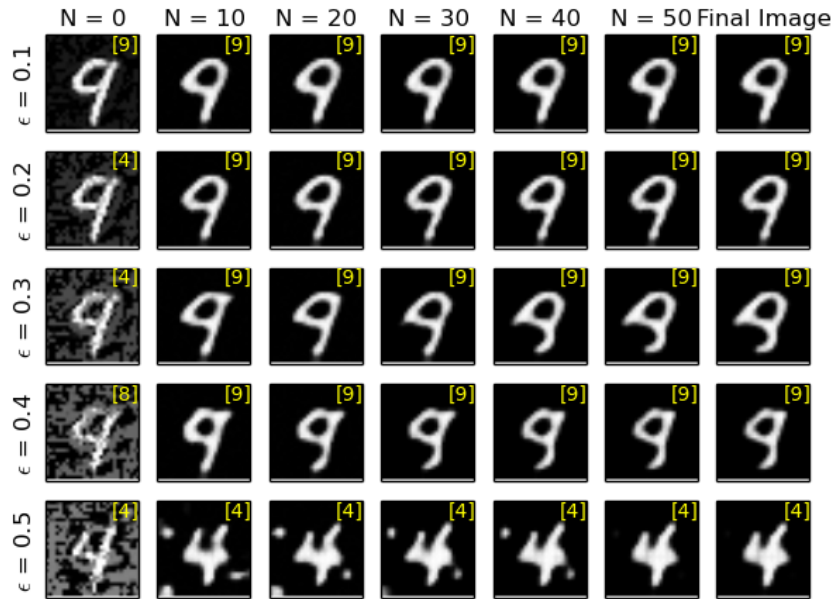


(b)

Figure 18: Sample images for the MALADE algorithm against a BPDAwEOT attack with L_∞ norm are shown here. The rows indicate the norm of the perturbation used by the attacked while the columns indicate the intermittent steps taken by MALADE to defend the attack. The classifier’s decision is displayed in yellow in the top right corner of each image. Since the gradients are computed only until the input to the classifier, there is no gradient obfuscation and hence the attack is strong.

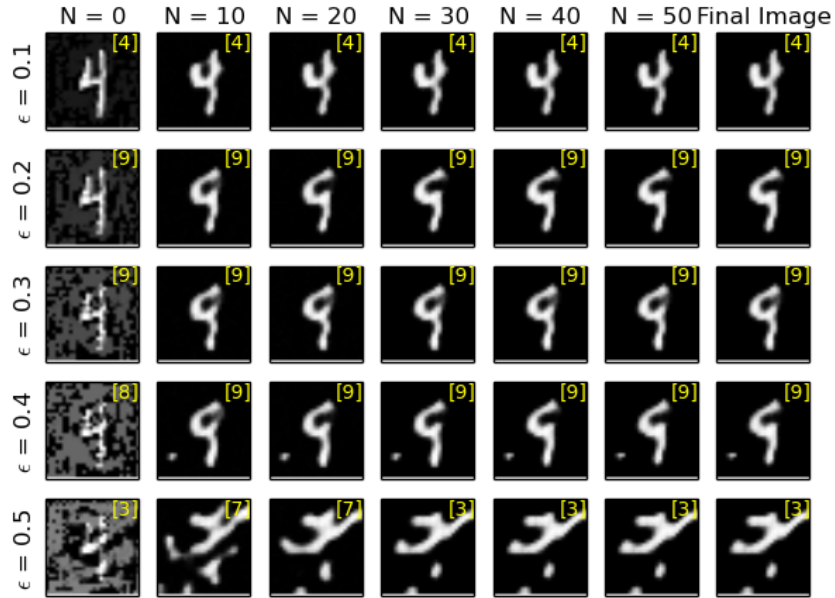


(a)

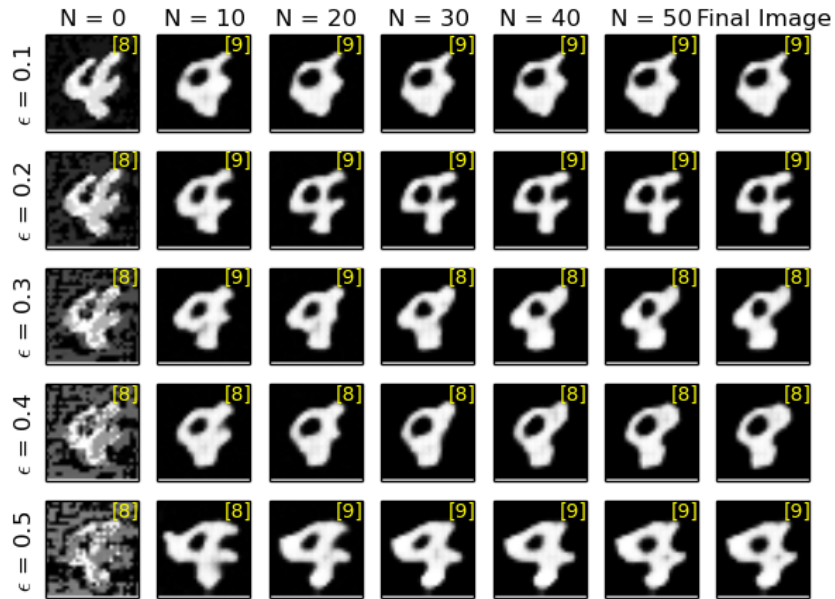


(b)

Figure 19: Sample images for the MALADE algorithm against a BPDawEOT attack with L_∞ norm are shown here. The rows indicate the norm of the perturbation used by the attacked while the columns indicate the intermittent steps taken by MALADE to defend the attack. The classifier's decision is displayed in yellow in the top right corner of each image.



(a)



(b)

Figure 20: Sample images for the MALADE algorithm against a BPDAwEOT attack with L_∞ norm are shown here. The rows indicate the norm of the perturbation used by the attacked while the columns indicate the intermittent steps taken by MALADE to defend the attack. The classifier’s decision is displayed in yellow in the top right corner of each image.